Cell Stem Cell

Short Article

Reengineering an Antiarrhythmic Drug Using Patient hiPSC Cardiomyocytes to Improve Therapeutic Potential and Reduce Toxicity

Graphical Abstract

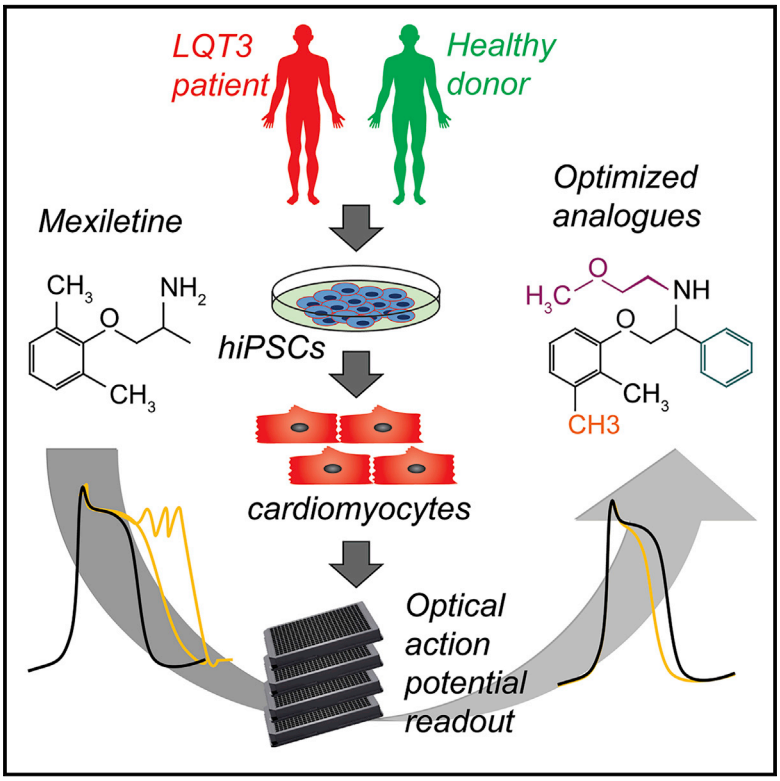

Authors

Wesley L. McKeithan, Dries A.M. Feyen, Arne A.N. Bruyneel, ..., Robert S. Kass, John R. Cashman, Mark Mercola

Correspondence

mmercola@stanford.edu

In Brief

McKeithan et al. used large-scale functional screening of hiPSC cardiomyocytes carrying a mutation that causes an electrophysiological disorder (long QT syndrome type 3) to direct the chemical optimization of mexiletine, an antiarrhythmic drug used to treat the disease. Four new analogs have greater potency and less proarrhythmic liability relative to mexiletine.

Highlights

- LQT3 hiPSC cardiomyocytes recapitulate disease phenotypes and drug responses
- Large-scale functional screens using LQT3 hiPSC-CMs enable drug optimization
- Optimized mexiletine analogs decrease proarrhythmic liability and improve potency

McKeithan et al., 2020, Cell Stem Cell *27*, 1–9
November 5, 2020
https://doi.org/10.1016/j.stem.2020.08.003

CellPress

Cell Stem Cell

CellPress

Short Article

Reengineering an Antiarrhythmic Drug Using Patient hiPSC Cardiomyocytes to Improve Therapeutic Potential and Reduce Toxicity

Wesley L. McKeithan,[1,2] Dries A.M. Feyen,[1] Arne A.N. Bruyneel,[1] Karl J. Okolotowicz,[3] Daniel A. Ryan,[3] Kevin J. Sampson,[4] Franck Potet,[5] Alex Savchenko,[1] Jorge Gómez-Galeno,[3] Michelle Vu,[1] Ricardo Serrano,[1] Alfred L. George, Jr.,[5] Robert S. Kass,[4] John R. Cashman,[3] and Mark Mercola[1,2,6,*]

[1]Cardiovascular Institute and Department of Medicine, Stanford University, Stanford, CA 94305, USA
[2]Graduate School of Biomedical Sciences, Sanford Burnham Prebys Medical Discovery Institute, San Diego, CA 92037, USA
[3]Human BioMolecular Research Institute, San Diego, CA 92121, USA
[4]Department of Pharmacology, College of Physicians and Surgeons, Columbia University, New York, NY 10032, USA
[5]Department of Pharmacology, Feinberg School of Medicine, Northwestern University, Chicago, IL 60611, USA
[6]Lead Contact
*Correspondence: mmercola@stanford.edu
https://doi.org/10.1016/j.stem.2020.08.003

SUMMARY

Modeling cardiac disorders with human induced pluripotent stem cell (hiPSC)-derived cardiomyocytes is a new paradigm for preclinical testing of candidate therapeutics. However, disease-relevant physiological assays can be complex, and the use of hiPSC-cardiomyocyte models of congenital disease phenotypes for guiding large-scale screening and medicinal chemistry have not been shown. We report chemical refinement of the antiarrhythmic drug mexiletine via high-throughput screening of hiPSC-CMs derived from patients with the cardiac rhythm disorder long QT syndrome 3 (LQT3) carrying SCN5A sodium channel variants. Using iterative cycles of medicinal chemistry synthesis and testing, we identified drug analogs with increased potency and selectivity for inhibiting late sodium current across a panel of 7 LQT3 sodium channel variants and suppressing arrhythmic activity across multiple genetic and pharmacological hiPSC-CM models of LQT3 with diverse backgrounds. These mexiletine analogs can be exploited as mechanistic probes and for clinical development.

INTRODUCTION

Somatic cells derived from human induced pluripotent stem cells (hiPSCs) have been shown to recapitulate a range of disease phenotypes *in vitro* (Matsa et al., 2016; Tiscornia et al., 2011). By reproducing human pathophysiology, hiPSC-based models have been considered a new paradigm for the development of precision therapeutics that target specific disease mechanisms. Despite the immense promise of disease-specific hiPSC models, only a few large-scale drug development efforts have used hiPSCs, and these studies were restricted to healthy donors (Hnatiuk and Mercola, 2019). Here, we describe the use of high-throughput physiological screening for arrhythmic phenotypes in hiPSC-derived cardiomyocytes (hiPSC-CMs) from patients with long QT syndrome type 3 (LQT3) to facilitate the rapid medicinal chemical refinement of a small-molecule drug, mexiletine.

Mexiletine is an orally available inhibitor of muscle and neuronal sodium channels. It is a class 1B antiarrhythmic drug (Singh et al., 2020) that is used to suppress life-threatening ventricular arrhythmia and to shorten the heart rate corrected QT interval (QTc) in LQT3 patients (Al-Khatib et al., 2018; Priori et al., 2015). The cardiac ventricular action potential (AP) is initiated by opening of sodium channels (e.g., $Na_v1.5$) to conduct a large inward Na^+ current (peak Na^+ current [I_{NaP}]) that drives rapid conduction in the ventricles. Most $Na_v1.5$ channels rapidly inactivate with depolarization, but a small subset of channels fails to inactivate and mediate late Na^+ current (I_{NaL}). LQT3 is caused by mutations in the pore-forming α subunit of $Na_v1.5$ (encoded by *SCN5A*) that impair channel inactivation and accelerate recovery from the inactivated state, increasing I_{NaL} to oppose repolarization and prolong the AP. These cellular effects prolong the QT interval on the surface electrocardiogram. LQT3 affects children and teenagers, is characterized by episodes of polymorphic ventricular tachycardia, and carries a risk of sudden cardiac death. Mexiletine was shown to shorten the QTc in LQT3 patients (Schwartz et al., 1995) and subsequently to decrease the risk of ventricular tachycardia and ventricular fibrillation upon 35-month median follow-up (Mazzanti et al., 2016). Accordingly, mexiletine is included in current guidelines for treatment of LQT3, in addition to β-blockers and other antiarrhythmic drugs (Al-Khatib et al., 2018; Priori et al., 2015).In addition to LQT3, selective inhibition of I_{NaL} is considered a therapeutic strategy to treat electrical and contractile dysfunction in heart failure and cardiac ischemia (Horvath and Bers, 2014; Maier and Sossalla, 2013). Mexiletine is modestly selective for I_{NaL} over I_{NaP} but

Please cite this article in press as: McKeithan et al., Reengineering an Antiarrhythmic Drug Using Patient hiPSC Cardiomyocytes to Improve Therapeutic Potential and Reduce Toxicity, Cell Stem Cell (2020), https://doi.org/10.1016/j.stem.2020.08.003

also inhibits the repolarizing K^+ current (I_{Kr}), prolongs cardiac AP, and promotes early afterdepolarizations (EADs) *in vitro* at concentrations near the therapeutic plasma concentration and IC_{50} for inhibition of I_{NaL} (Gualdani et al., 2015; McKeithan et al., 2017). It is unknown whether the therapeutic and proarrhythmic properties of mexiletine result from -chemical moieties that dictate inhibition of I_{NaL} or from other unrelated determinants. Studies of the skeletal muscle Na^+ channel $Na_v1.4$ (encoded by *SCN4A*) and $Na_v1.5$ have shown that chemical substituents near the mexiletine center of chirality strongly modulate potency for inhibition of Na^+ current (I_{Na}) (De Bellis et al., 2013; De Luca et al., 2000, 2003; Roselli et al., 2016). To explore a large number of chemical modifications, we took advantage of high-throughput physiological screening in hiPSC-CMs. The human CM context is advantageous over simpler systems because it includes not only the $Na_v1.5$ pore-forming α subunit but also ancillary proteins that regulate channel function. Furthermore, screening for a complex phenotype such as AP morphology in this context is unbiased with respect to target protein or molecular mechanism of action.

Based on the electrophysiological responses of LQT3 and healthy hiPSC-CMs, we identified structural analogs of mexiletine with greater potency and selectivity for I_{NaL} that decreased AP prolongation and suppressed EADs. The analogs effectively suppressed arrhythmia in spontaneous genetic and pharmacologically induced hiPSC-CM models of LQT3 from multiple genetic backgrounds. These studies illustrate the potential of using complex physiological models of patient-derived hiPSC-CMs for precision drug design.

RESULTS

hiPSC-CM Generation and Development of High-Throughput Assays

hiPSC-CMs were generated from a previously characterized LQT3 patient harboring a *de novo* F1473C missense *SCN5A* mutation that presented with a QTc of 825 ms and 2:1 atrioventricular (AV) block (Bankston et al., 2007; Silver et al., 2009; Terrenoire et al., 2013). The patient tolerated a high dose (24 mg/kg/day) of mexiletine that provided partial control of his arrhythmia. To conduct the high-throughput screen, we used LQT3 SCN5A F1473C hiPSC-CMs derived from this individual and prepared by Cellular Dynamics International (CDI) (MyCell Cardiomyocytes; see STAR Methods), as well as commercially available healthy donor hiPSC-CMs (iCell Cardiomyocytes, termed herein HD.CDI). Our previous studies showed that these hiPSC-CMs, generated by CDI, as well as an independent hiPSC derivation, showed elevated I_{NaL} (relative to healthy controls) that was inhibitable by mexiletine (McKeithan et al., 2017; Terrenoire et al., 2013). In the high-throughput screen, there was variation in the action potential duration at 75% repolarization (APD_{75}) and the spontaneous beat rate that depended on the particular sample of hiPSC-CMs (Figures S1A–S1C). Despite this variation, LQT3 hiPSC-CMs showed characteristic AP prolongation relative to healthy donor controls when corrected for beat rate (Fridericia, 2003; Figures 1B, 1D, and S1D) and a dose-dependent shortening of the APD in response to mexiletine (EC_{50} = ~5 μM) (Figures 1A and 1B) that was highly reproducible across experiments (Figures S1E–S1E″). Interestingly, the LQT3 hiPSC-CMs showed only modest APD prolongation (~100 ms) at high doses of mexiletine (Figures 1A, 1B, and S1E–S1E″) consistent with the patient's tolerance of high-dose mexiletine therapy (Bankston et al., 2007; Silver et al., 2009; Terrenoire et al., 2013). In contrast, HD.CDI hiPSC-CMs showed a proarrhythmic response to mexiletine (Figures 1C, 1D, and S1F–S1F″). hiPSC-CMs from three unrelated healthy donors (HD.15S1, HD.113, and HD.273) with a normal *SCN5A* sequence also showed proarrhythmic responses (Figure 1C). None of the healthy donor lines exhibited APD shortening in response to mexiletine. Therefore, we used the LQT3 SCN5A F1473C hiPSC-CMs to screen for APD shortening and HD.CDI hiPSC-CMs to detect APD prolongation and EADs (Figure 1E). As a positive control for the proarrhythmic phenotype, experiments included hiPSC-CMs treated with dofetilide, a selective I_{Kr} inhibitor, that prolonged the AP and induced EADs in HD.CDI and LQT3 iPSC-CMs (EC_{50} = 4–7 nM) (Figures S1G–S1G″ and S1H–S1H″), as well as the Na^+ channel blocker tetrodotoxin (TTX) to confirm dependence on I_{Na} for AP generation of the SCN5A F1473C hiPSC-CMs (EC_{50} = 3.6 μM) (Figures S1I–S1I″). The effects of mexiletine, dofetilide, and TTX on AP kinetics were highly reproducible across experiments (Figures S1E″–S1I″).

Physiological Screening and Mexiletine Reengineering

We implemented a strategy (Figure 1E) using the LQT3 (SCN5A F1473C) patient and HD.CDI hiPSC-CMs to characterize the effect of mexiletine analogs on APD shortening and proarrhythmic phenotypes by high-throughput optical recording of APs. Analogues that shortened the APD in the SCN5A F1473C hiPSC-CMs were tested using automated planar patch clamp to directly measure inhibition of I_{Na} and I_{Kr}. Analogues were synthesized and analyzed iteratively (Figure 2A). Phenyl mexiletine **MexA1** (Figure 2B) was tested, because bulky substitutions at the alpha position to the amine of mexiletine had previously been shown to increase potency for I_{Na} inhibition in skeletal and cardiac muscle voltage-gated Na^+ channels (De Bellis et al., 2013; De Luca et al., 2000, 2003; Roselli et al., 2016). **MexA1** increased the potency of APD shortening in SCN5A F1473C hiPSC-CMs with efficacy similar to that of mexiletine while decreasing induction of EADs. The results are summarized in Figure 2C, and representative AP recordings are shown in Figures S2A and S2C. Automated planar patch-clamp studies confirmed that **MexA1** had increased potency against I_{Na} and I_{Kr} relative to mexiletine but also showed a loss of selectivity for I_{NaL} over I_{NaP} (Table S1).

Given that **MexA1** was more potent but less selective than mexiletine, we sought to restore selectivity for I_{NaL}. Three modifications to the phenoxy region on the opposite side of the molecule, the *ortho* mono-substituted methyl (**MexA2**), 3,5-dimethyl (**MexA3**), and *ortho* trifluoromethyl-substituted (**MexA4**) analogs, potently shortened APD in SCN5A F1473C hiPSC-CMs (Figures 2B, 2C, S2A, and S2B). **MexA2**, **MexA3**, and **MexA4** were not proarrhythmic in HD.CDI hiPSC-CMs at any dose examined (Figures 2C, S2C, and S2D). **MexA2**, **MexA3**, and **MexA4** were extremely potent against I_{NaL} ($IC_{50} \leq 1$ μM) and were more selective than mexiletine for inhibition of I_{NaL} over I_{NaP} (selectivity ratios were 53.4, 100.5, and 39.5, respectively, compared with 1.8 for **MexA1** and 8.3 for mexiletine; see Table S1 and Figures S2E–S2I). **MexA2**, **MexA3**, and **MexA4** were also more selective for I_{NaL} over I_{Kr} (ratios were >31 for

Please cite this article in press as: McKeithan et al., Reengineering an Antiarrhythmic Drug Using Patient hiPSC Cardiomyocytes to Improve Therapeutic Potential and Reduce Toxicity, Cell Stem Cell (2020), https://doi.org/10.1016/j.stem.2020.08.003

CellPress

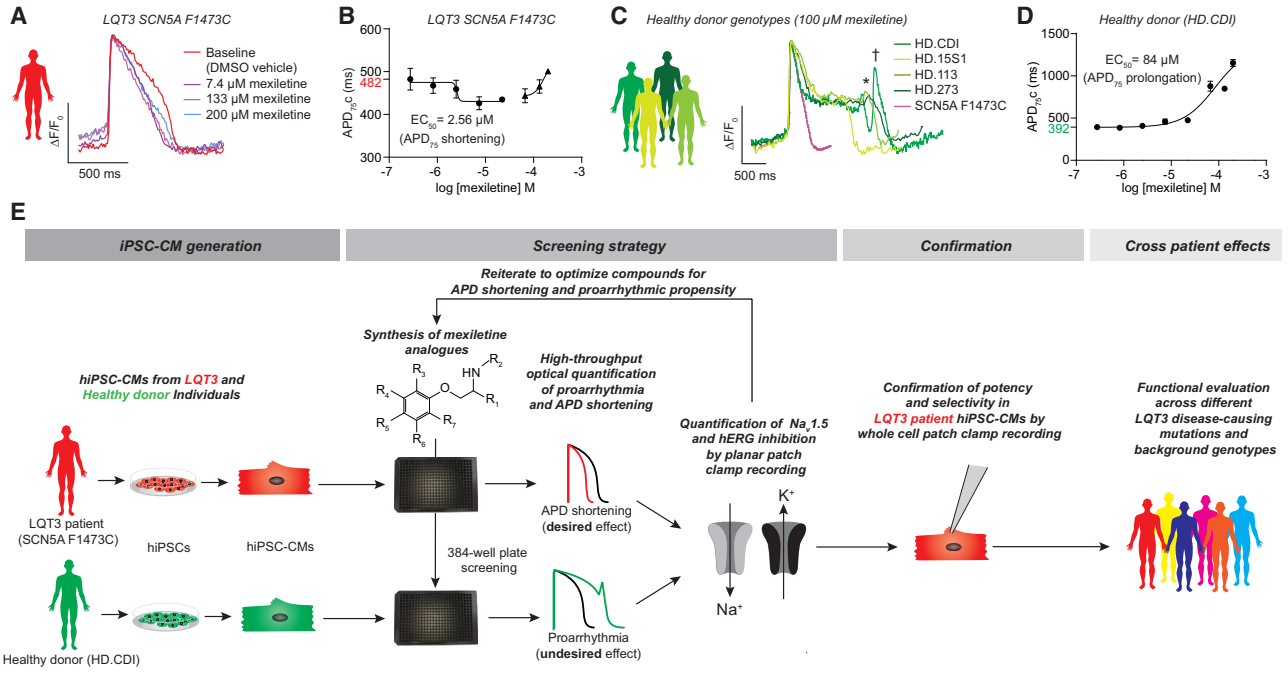

Figure 1. Phenotypic Screening Based on Physiological Response of hiPSC-CMs

(A and B) On-target phenotype. Representative optical AP traces show dose-dependent shortening of AP duration in response to mexiletine in LQT3 SCN5A F1473C hiPSC-CMs (A) and a dose-response curve for spontaneous beat rate corrected APD_{75} shortening in SCN5A F1473C hiPSC-CMs (B). The baseline APD_{75} of 482 ms is shown in red (B).

(C and D) Off-target phenotype. Representative optical AP traces show dose-dependent prolongation of AP duration in response to mexiletine in healthy donor hiPSC-CMs (C). *EADs (HD.113 trace); †delayed afterdepolarizations (DADs) (HD.CDI trace). A dose-response curve for spontaneous beat rate corrected APD_{75} prolongation in healthy donor hiPSCs (HD.CDI) (D). The baseline APD_{75} of 392 ms is shown in green (D).

(E) Drug reengineering strategy. hiPSC-CMs were generated from cells of an LQT3 patient and a healthy donor. Iterative cycles of chemical syntheses, optical high-throughput screening, and (in selected compounds) assessment of I_{Na} and K^+ current inhibition using automated planar patch-clamp assays resulted in a set of lead candidates. Following confirmation of I_{Na} inhibition in LQT3 hiPSC-CMs, compounds were tested for efficacy against a panel of LQT3 disease-causing mutations to assess the influence of mutation and individual human genetic background on compound responsiveness.

Data points in (B) and (D) indicate mean ± SEM, n = 3.

MexA2–MexA4, compared with 0.7 for **MexA1** and 2.5 for mexiletine; see Table S1 and Figures S2J–S2N). Less I_{Kr} block is desirable, because it is a well-recognized mechanism of drug-induced proarrhythmia. The analogs, in particular **MexA3** and **MexA4**, caused asystole at concentrations above 66 μM in both LQT3 and healthy donor hiPSC-CMs. Probing the chemical basis for asystole, we observed that N-ethyl methoxy substitution on the primary amine decreased this effect, as exemplified by **MexA5** (Figures 2B and 2C).

Validation of Function in LQT3 Patient hiPSC-CMs

To verify function in a CM context, mexiletine analogs were tested for their electrophysiological effects on I_{NaL} and I_{NaP} by whole-cell patch-clamp recording of LQT3 SCN5A F1473C hiPSC-CMs (Figures 2E–2I; Table S2). As in the heterologous expression system, **MexA2–MexA5** were more potent (28.3- to 134-fold) and selective (22.3- to 117-fold) than mexiletine in inhibiting I_{NaL} relative to I_{NaP} in LQT3 CMs.

In summary (Figure 2D), introduction of a phenyl group alpha to the primary amine (**MexA1**) increased potency for APD shortening and decreased proarrhythmic liability but also abrogated selectivity for inhibition of I_{NaL} over I_{NaP}. Introduction of substituents to the phenoxy moiety (i.e., **MexA2–MexA5**) restored selectivity for I_{NaL} over I_{NaP} inhibition, whereas N-ethyl methoxy substitution (**MexA5**) decreased the asystolic effect observed at high concentrations of non-N-substituted phenyl mexiletine derivatives.

Evaluation of MexA2–MexA5 against LQT3-Causing SCN5A Mutations

Given the diversity of SCN5A mutations causing LQT3, we tested I_{NaP} and I_{NaL} inhibition of **MexA2–MexA5** across a panel of 7 LQT3-causing mutant channels, including F1473C, expressed in HEK293T cells by automated planar patch clamp (Figure 3A). To compare efficacy against the panel of channels, each compound was tested at a single dose corresponding to the EC_{80} for the F1473C mutant channel (Figures 3B and 3C). Normalization of the dataset by analog revealed differential inhibition profiles (Figure 3D). The compounds were generally effective against all mutant channels examined with the exception of **MexA2** and **MexA3**, which did not block I_{NaL} in the L409P/R588 mutant (Figures 3B, 3C, S2O, and S2P). Among all mutants

Please cite this article in press as: McKeithan et al., Reengineering an Antiarrhythmic Drug Using Patient hiPSC Cardiomyocytes to Improve Therapeutic Potential and Reduce Toxicity, Cell Stem Cell (2020), https://doi.org/10.1016/j.stem.2020.08.003

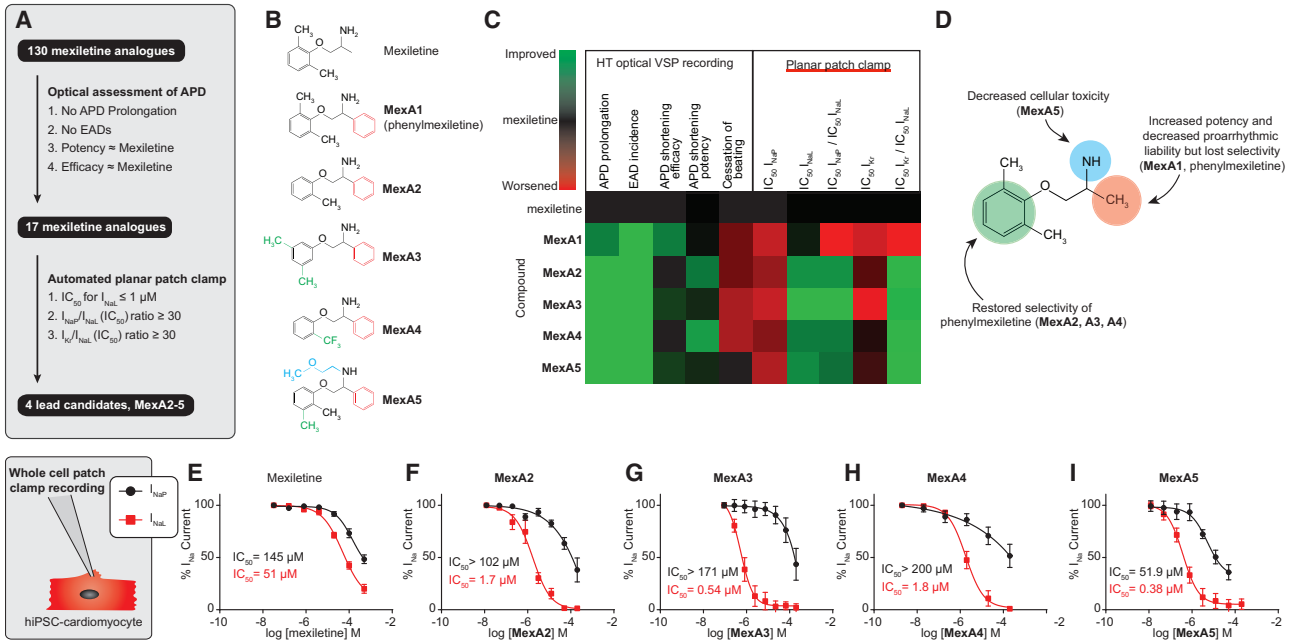

Figure 2. Distinct Chemical Substituents Discriminate the Therapeutic and Proarrhythmic Effects of Mexiletine on hiPSC-CMs AP Kinetics

(A) Compound triage. Analogues were screened through multiple cycles of synthesis and optical testing as in Figure 1E. Analogues that passed initial screen criteria were assessed for specific effects on I_{Na} and K^+ current (I_K), ultimately resulting in 4 lead candidates.

(B) Chemical structures of mexiletine, phenyl mexiletine (**MexA1**), and lead candidates (**MexA2–MexA5**).

(C) Heatmap representation of physiological responses of mexiletine and phenyl mexiletine analogs. Scale: green is improved and red is worse relative to mexiletine (black). See Figure S2 and Table S1 for numerical data. **MexA1** showed a favorable decrease in APD prolongation and EAD incidence (arrhythmia phenotypes) but worse selectivity ratios for I_{NaL} relative to mexiletine. Selectivity was restored by phenoxy substitutions (**MexA2–MexA5**).

(D) Summary of the phenotypic effects of chemical modifications to mexiletine.

(E–I) Dose-dependent effects on I_{NaP} and I_{NaL} in LQT3 SCN5A F1473C hiPSC-CMs by whole-cell patch-clamp recording. Data are represented as mean ± SEM, n = 4. See Table S2 for a numerical summary.

examined, **MexA2–MexA5** were most effective against I_{NaL} in F1473C and delKPQ (Figure 3D). Selectivity for F1473C might be expected, because it was used in the primary screening.

Effect of Mexiletine Analogs in hiPSC-CM Models of LQT3

To gauge effectiveness in hiPSC-CMs from different individuals, we tested **MexA2** in a second genetic LQT3 model with a distinct mutation in SCN5A (N406K) (Spencer et al., 2014) that is mexiletine responsive (Hu et al., 2018). In these and subsequent studies, the hiPSC-CMs were prepared using a metabolic maturation protocol (Feyen et al., 2020; STAR Methods). Because wild-type SCN5A is less responsive to mexiletine (Hu et al., 2018; Zhu et al., 2019), we also created pharmacological models of LQT3 by treating two healthy donor hiPSC-CMs (HD.15S1 and HD.113) with veratridine (0.37 μM) to cause persistent activation and ATX-II (0.5 μM) to inhibit inactivation of $Na_v1.5$ (Figure 4A). For comparison, we also tested I_{NaL} inhibitors GS945867 (GS-967) (Koltun et al., 2016) and ranolazine. Both are selective blockers of I_{NaL} over I_{NaP} but are structurally distinct from each other and mexiletine (Zablocki et al., 2016).

Mexiletine shortened APD at intermediate doses in LQT3 SCN5A F1473C and weakly in LQT3 SCN5A N406K (Figures 4B–4G, S3A, and S3B), but not in all pharmacological models (Figures 4H–4P and S3C–S3E). At higher doses, mexiletine substantially prolonged the AP in all hiPSC-CMs examined, often inducing EADs, except in LQT3 SCN5A F1473C. This finding was consistent with earlier results (Figure 1A). In contrast, **MexA2** shortened APD across all genetic and pharmacological LQT3 models without prolongation (Figures 4B–4P and S3A–S3E). **MexA5** showed similar efficacy to **MexA2** in shortening the APD of genetic and pharmacological LQT3 models (Figures S4B–S4I). The other I_{NaL} blockers showed mutation-specific efficacy. For instance, ranolazine shortened APD without prolongation at high doses in LQT3 SCN5A F1473C hiPSC-CMs but did not shorten APD and induced EADs at high doses in LQT3 SCN5A N406K hiPSC-CMs (Figures 4B–4G, S3A, and S3B). In general, **MexA2**, **MexA5**, and GS-967 showed the most pronounced shortening at low doses, whereas mexiletine and ranolazine prolonged the APD at high doses (Figures 4B–4P, S3A–S3E, and S4B–S4I).

Effect of MexA2 on Suppression of Arrhythmia

We tested the ability of **MexA2, MexA5**, and other I_{NaL} inhibitors to suppress spontaneous arrhythmias that arise in about half of SCN5A N406K hiPSC-CM differentiations, as well as a high-dose ATX-II-induced arrhythmia in healthy donor hiPSC-CMs (Figures 4Q, S3F, S3G, and S4J–S4M). Both **MexA2** and **MexA5** terminated spontaneous arrhythmias in SCN5A N406K hiPSC-CMs. **MexA2** terminated arrhythmia at 3-fold lower doses than mexiletine in the SCN5A N406K and ATX-II models. GS-967

Please cite this article in press as: McKeithan et al., Reengineering an Antiarrhythmic Drug Using Patient hiPSC Cardiomyocytes to Improve Therapeutic Potential and Reduce Toxicity, Cell Stem Cell (2020), https://doi.org/10.1016/j.stem.2020.08.003

CellPress

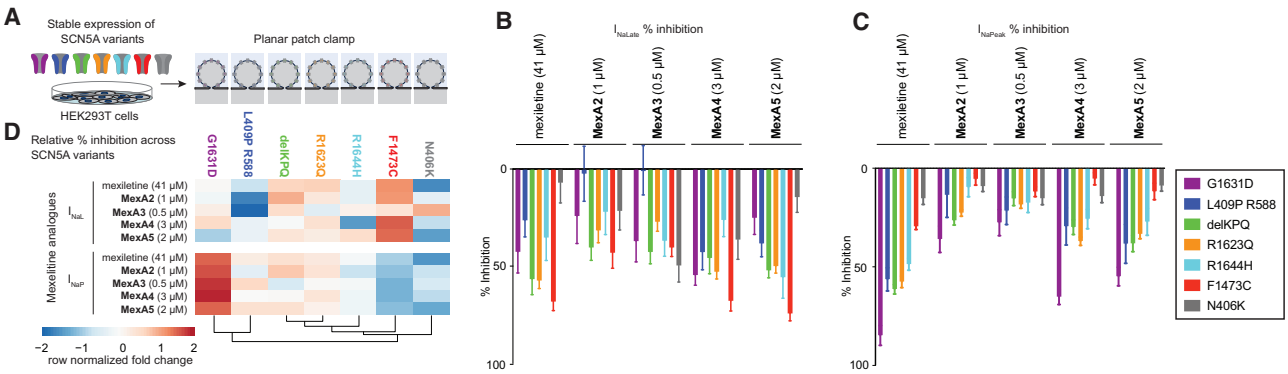

Figure 3. Effects of *SCN5A* Variants on Responsiveness to Mexiletine and Phenyl Mexiletine Analogs

(A) Schematic of seven *SCN5A* variants transiently expressed in HEK293T cells and analyzed by planar patch-clamp recording.

(B and C) Mean percentage of inhibition ± SEM of I_{NaL} and I_{NaP} inhibition. Each analog was evaluated at a single dose (EC_{80} for SCN5A F1473C from Figures S2E–S2I and Table S1). See Figures S2O and S2P for individual data points.

(D) Normalization of mean percentage of inhibition by analog (row normalization in the heatmap representation) portraying compound-specific profiles of inhibition across the *SCN5A* mutants.

was effective, but ranolazine blocked arrhythmia only in the genetic LQT3 model (SCN5A N406K). In summary, **MexA2** and **MexA5** potently reverted LQT3 phenotypes in hiPSC-CMs of different genotypes and LQT3-causing SCN5A mutations.

DISCUSSION

We described the iterative chemical refinement of mexiletine analogs based on their effects on desirable AP shortening, unwanted AP prolongation, and EAD phenotypes in hiPSC-CMs. Our study demonstrates that a disease phenotype of patient-derived hiPSC-CMs can guide the improvement and optimization of a drug. We succeeded in identifying four mexiletine analogs (**MexA2**–**MexA5**) that did not induce AP prolongation or EADs and yet retained the ability to suppress arrhythmia in hiPSC-CM models of LQT3.

MexA2–**MexA5** were 28- to 134-fold more potent and 22- to 117-fold more selective in inhibiting I_{NaL} relative to I_{NaP} compared with mexiletine in SCN5A F1473C hiPSC-CMs. These compounds also showed greatly improved selectivity for I_{NaL} relative to I_{Kr} inhibition (>31-fold) compared with mexiletine. However, they retained comparable I_{Kr} inhibition to mexiletine. This finding implies that another mechanism is responsible for the absence of AP prolongation and EADs. Thus, conventional planar patch screening for I_{Na} and I_{Kr} block (Table S1) as logical determinants of AP prolongation and EAD propensity would not have predicted the absence of AP prolongation and EADs upon treatment with high doses of **MexA2**–**MexA5**. AP waveforms depend on a complex interplay of multiple ion channels. Our results illustrate the advantages of directly screening for alterations in hiPSC-CM AP waveform morphology when investigating the chemical basis for complex electrophysiological phenotypes such as EADs, rather than relying on effects on individual channel types in non-CM overexpression systems.

More than 750 *SCN5A* mutations have been reported, of which 227 have been associated with LQT3 (Stenson et al., 2017). Individual mutant channels respond differently to mexiletine (Ruan et al., 2007, 2010). In addition to F1473C, **MexA2**–**MexA5** were tested against six LQT3-causing mutant channels expressed in HEK293 cells to eliminate the influence of genetic background (Figure 3). **MexA2**–**MexA5** blocked five of the seven SCN5A mutant channels, demonstrating broad efficacy against multiple mutations, albeit with subtle mutation-specific effects (Figure 3D). **MexA2**–**MexA5** were uniformly effective at inhibiting I_{NaL} mediated by SCN5A F1473C mutant channels (Figure 3D), suggesting that reliance on a single variant in primary screening might bias the development of therapeutics in favor of individuals carrying that variant. A channel with a missense mutation (i.e., L409P) combined with a common genetic variant (i.e., R588) was inhibited by mexiletine and two analogs (**MexA4** and **MexA5**), but not by two others (**MexA2** and **MexA3**). This channel is responsible for a highly malignant LQT3 phenotype that was originally detected *in utero* and is resistant to block by lidocaine that binds to the same site as mexiletine in $Na_v1.5$ (Murphy et al., 2012). The mechanism of resistance is unclear but might reflect alterations in biophysical properties of $Na_v1.5$ (e.g., ultra-rapid recovery from inactivation and shift of steady-state inactivation to depolarized voltage potentials) (Murphy et al., 2012). Interestingly, **MexA2** and **MexA3** preferentially blocked I_{NaP} over I_{NaL}, which may point to a unique interaction between these compounds and the channel mutants. More generally, the structural basis for variable effectiveness of mexiletine is of considerable research and clinical interest. Current models hold that mexiletine preferentially binds with greatest affinity when the channel is in its inactivated state (Desaphy et al., 2001). LQT3 mutations that increase the persistence of the inactivated state (that occurs when the channel's inactivation gate blocks access to the pore) correlate with the efficacy of QT interval shortening in patients (Ruan et al., 2007). Other mutation-induced conformational changes in the channel modulate drug responsiveness. For instance, Zhu et al. (2019) proposed, based on mutational analysis, that the activated conformation of the domain III voltage-sensing domain of the α subunit (DIII-VSD) enhances mexiletine binding and inhibition. Mexiletine docking to the channel pore maintains the DIII-VSD in an activated conformation (Zhu et al., 2019). The mexiletine analogs described

Please cite this article in press as: McKeithan et al., Reengineering an Antiarrhythmic Drug Using Patient hiPSC Cardiomyocytes to Improve Therapeutic Potential and Reduce Toxicity, Cell Stem Cell (2020), https://doi.org/10.1016/j.stem.2020.08.003

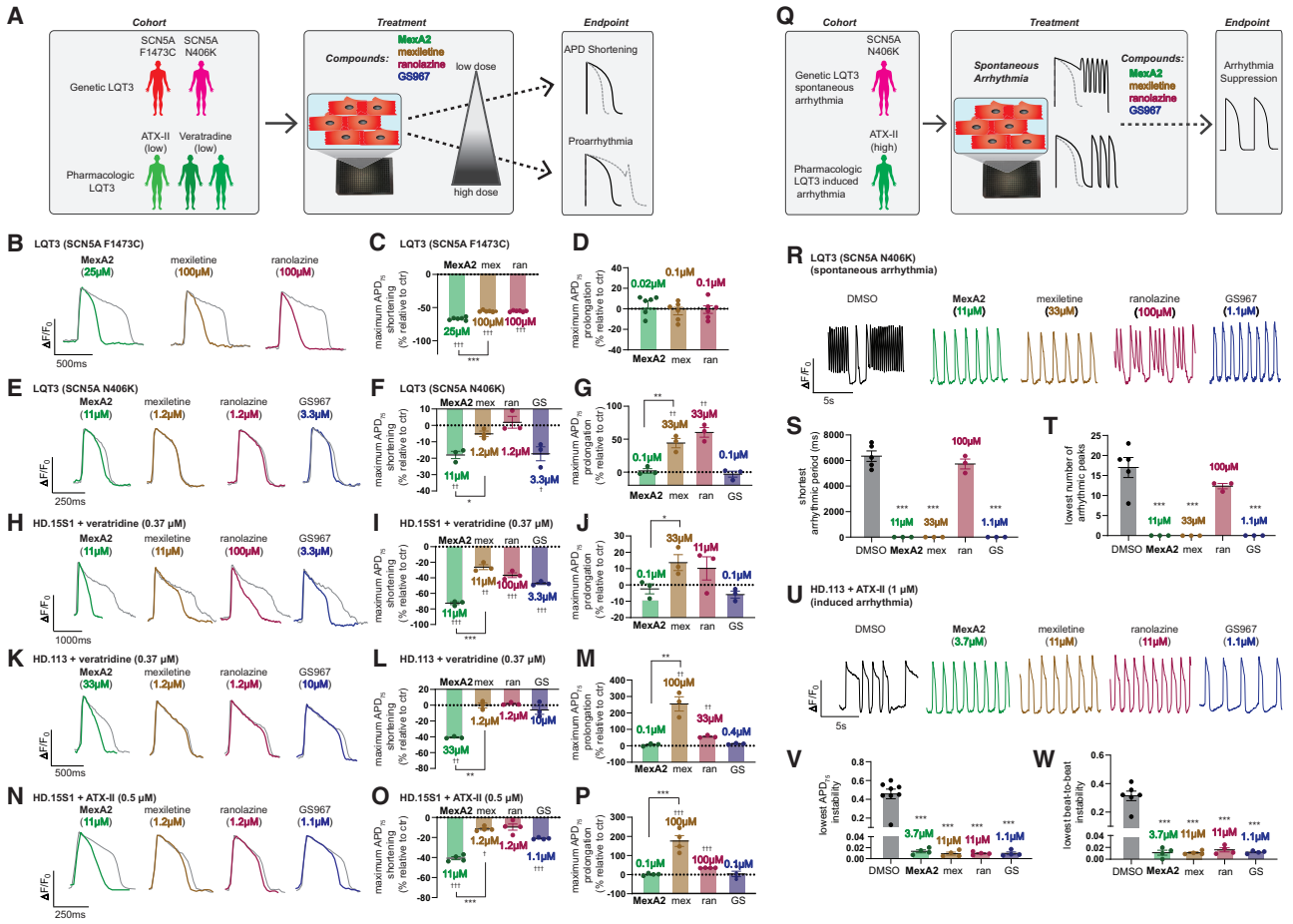

Figure 4. Relative Therapeutic Efficacy of MexA2 and I_{NaL} Inhibitors in a Cohort of LQT3 hiPSC-CM Models Reflecting Different Human Genetic Backgrounds and Disease Manifestations

(A) Experimental setup to test the therapeutic efficacy and toxicity of **MexA2** and other I_{NaL} blockers in genetic and pharmacological LQT3 hiPSC-CM models.

(B–G) Genetic models of LQT3 in hiPSC-CMs. Representative optical voltage recordings of APs from individual compounds at the lowest dose with the maximum APD_{75} shortening effect (B and E). Each trace is an average normalized $\Delta F/F_0$ versus time plot (33 Hz) from multiple peaks in a well (n = 3–5 peaks). The gray lines represent AP recording from respective control wells. Maximum APD_{75} shortening (C and F) and prolongation (D and G) attained by each compound in individual models of LQT3. APD_{75} shortening and prolongation times (in milliseconds) are represented as the change from their respective control wells (n = 3–6 wells). Data are represented as mean ± SEM.

(H–P) Pharmacological models of LQT3 in hiPSC-CMs. Representative optical voltage recordings of APs from individual compounds at the lowest dose with the maximum APD_{75} shortening effect (H, K, and N). Each trace is an average normalized $\Delta F/F_0$ versus time plot (33 Hz) from multiple peaks in each well (n = 3–5 peaks). The gray lines represent AP recording from respective control wells. Maximum APD_{75} shortening (I, L, and O) and prolongation (J, M, and P) attained by each compound in each model of LQT3. APD_{75} shortening and prolongation times (in milliseconds) are represented as the change from their respective control wells (n = 3–6 wells).

(Q) Experimental setup for evaluating arrythmia suppression by small molecules. Genetic LQT3 SCN5A N406K hiPSC-CMs led to spontaneous arrythmias and a high dose of ATX-II (1 μM)-induced triggered activity in healthy donor (HD.113) hiPSC-CMs.

(R) Representative optical voltage recordings of AP in LQT3 SCN5A N406K hiPSC-CMs with spontaneous arrhythmia. An individual AP trace is shown for each compound at the lowest dose that attained the shortest arrhythmic period and lowest number of arrhythmic peaks (more information about metrics in Figure S4A).

(S and T) Graphs indicating the shortest arrhythmic period (S) and lowest number of arrhythmic peaks (T) attained by individual drugs (n = 3 wells).

(U) Representative optical voltage recording of the ATX-II (1 μM)-induced arrythmia in HD.113 hiPSC-CMs for each compound at the lowest dose that achieved maximal reversion of APD_{75} instability and beat-to-beat instability (instability = standard deviation/mean).

(V and W) Quantification of ATX-II-induced arrythmia and the lowest dose that achieved maximal suppression of APD_{75} instability (V) and beat-to-beat instability (W) for each compound (n = 3 wells).

Data are presented as mean ± SEM. Statistical significance was calculated by unpaired t test comparing either **MexA2** and mexiletine groups (*) or the individual compound versus untreated control (†) for (B)–(P). One-way ANOVA with Dunnett's method for multiple comparisons was used in (S), (T), (V), and (W) (versus the DMSO control group) (*). ††† and ***p < 0.001; †† and **p < 0.01; † and *p < 0.05. mex, mexiletine; ran, ranolazine; GS-967, GS.

Please cite this article in press as: McKeithan et al., Reengineering an Antiarrhythmic Drug Using Patient hiPSC Cardiomyocytes to Improve Therapeutic Potential and Reduce Toxicity, Cell Stem Cell (2020), https://doi.org/10.1016/j.stem.2020.08.003

herein that show variant selectivity might be useful tools to probe how mutations affect channel pharmacology.

Selective I_{NaL} inhibitors ranolazine and a clinical candidate related to GS-967 (GS-6615, eleclazine) were previously under clinical evaluation for LQT3 (Priori et al., 2018, Circulation, abstract). **MexA2** and **MexA5** compared favorably to these structurally distinct compounds for the ability to shorten APD and suppress spontaneous arrhythmia in both hiPSC-CM LQT3 genetic (SCN5A N406K) and pharmacological (ATX-II) models that reflect different mechanisms of impaired channel inactivation and patient backgrounds (Figure 4).

hiPSC modeling of genetic heart disease is an enabling technology for drug development, because it introduces aspects of the clinical presentation of disease into the earliest stages of the discovery and development pipeline. Precedents include predicting proarrhythmic and cardiotoxic responses to drugs and the discovery of small-molecule probes of diabetic cardiomyopathy and ischemic heart disease (Blinova et al., 2018; Drawnel et al., 2014; Fiedler et al., 2019; Sharma et al., 2017). We believe that the use of congenital disease models in large-scale screening or to guide medicinal chemistry is the next step for implementation of hiPSC-CMs in the drug discovery pipeline, and our study demonstrates the feasibility of this approach. There are several steps to translate these findings to drug development, including functional testing in a murine model (Fabritz et al., 2010; Nuyens et al., 2001; Schroder et al., 2014) or pharmacological model (e.g., ATX-II-treated *ex vivo* rabbit heart) (Belardinelli et al., 2013). These would be followed by pharmacokinetic, pharmacodynamic, and toxicity studies in large animals in anticipation of clinical testing.

In summary, we showed that patient-derived and pharmacological hiPSC-CM models can recapitulate the beneficial and adverse pharmacological effects of mexiletine. Through medicinal chemistry refinement, four phenyl mexiletine analogs (**MexA2**–**MexA5**) were found to have greater on-target potency and selectivity, in addition to decreased proarrhythmic liability, relative to mexiletine. These compounds were generally effective against different SCN5A mutations and suppressed arrhythmia in a cohort of hiPSC-CM LQT3 models reflective of distinct human genetic backgrounds. This study highlights the use of disease-specific hiPSCs in drug discovery. In particular, the results illustrate the use of hiPSC-derived models to develop small-molecule drugs based on the quantitative assessment of therapeutic potential and liabilities directly in a disease-relevant human cellular context.

Limitations of Study

Limitations of this study include the use of hiPSC-CMs that are relatively immature compared with adult CMs. CM immaturity might bias the development of compounds toward those that target proteins and processes that operate in early fetal CMs, rather than adult CMs. It would not have been possible to conduct a large-scale screen using adult human CMs; therefore, to help mitigate the limitations caused by physiological immaturity, we employed a metabolism-based maturation protocol that yielded hiPSC-CMs with Na^+-dependent APs (STAR Methods; Feyen et al., 2020). Key modifications to the media were low glucose and addition of oxidative energy substrates that resulted in a low resting membrane potential and fast depolarization (>200 V/s) because of the large inwardly rectifying K^+ current (I_{K1}) that sets the resting membrane potential and increases the number of activatable Na^+ channels. Although the Na^+ channel electrophysiology and cellular basis for arrhythmia are suitable for screening and initial characterization of compounds, the hiPSC-CM model does not fully replicate complex multicellular arrhythmia substrates. Therefore, additional evaluation of lead compounds for safety and efficacy for LQT3 or suppression of ventricular arrhythmia should be conducted in animal models (e.g., canine models) that have a similar electrophysiological basis for AP morphology and arrhythmia susceptibility as humans.

STAR★METHODS

Detailed methods are provided in the online version of this paper and include the following:

- KEY RESOURCES TABLE
- RESOURCE AVAILABILITY
  - Lead Contact
  - Materials availability
  - Data and Code Availability
- EXPERIMENTAL MODEL AND SUBJECT DETAILS
  - iCell Cardiomyocyte Culture (corresponds to Figure 2)
  - Differentiation of hiPSCs to cardiomyocytes (corresponds to Figure 4)
- METHOD DETAILS
  - High throughput optical action potential recording
  - Automated planar patch clamp
  - hiPSC-CM electrophysiology
  - Chemistry
  - Illustration of methods for the synthesis of compounds MexA2-5
- QUANTIFICATION AND STATISTICAL ANALYSIS

SUPPLEMENTAL INFORMATION

Supplemental Information can be found online at https://doi.org/10.1016/j.stem.2020.08.003.

ACKNOWLEDGMENTS

We thank J. Wu (Stanford Cardiovascular Institute, Stanford, CA) and the Stanford Biobank for the healthy donor hiPSC lines. We also thank B. Conklin (Gladstone Institute of Cardiovascular Disease) for the LQT3 SCN5A N406K hiPSC line and Tatiana Abramova (Northwestern University) for engineering and expressing mutant $Na_v1.5$ plasmid constructs. This research was made possible by grants from the National Institutes of Health (NIH R01HL113601, R01HL130840, R01HL141358, P01HL141084, and R21HL141019 to M.M.; U01 HL131914 to A.L.G.; and R01HL123483 to R.S.K.), the American Heart Association (9SFRN34820006 to A.L.G.), and the California Institute for Regenerative Medicine (CIRM grant TR4-06857 to J.R.C. and M.M.). The contents of this publication are solely the responsibility of the authors and do not necessarily represent the official view of CIRM or any other agency of the state of California. Flow cytometry and high-throughput screening services were supported by NIH P30CA030199 at the Sanford-Burnham-Prebys Medical Discovery Institute. This research was also supported by the Stanford Cardiovascular Institute and Stanford School of Medicine funds to M.M. D.A.M.F. was funded by the European Union's Horizon 2020 Research and Innovation Programme under Marie Sklodowska-Curie grant 708459. M.M. gratefully acknowledges funding from the Joan and Sanford Weill Scholarship Endowment.

AUTHOR CONTRIBUTIONS

Conceptualization, W.L.M., K.J.O., D.A.R., R.S.K., J.R.C., and M.M.; Methodology, W.L.M., D.A.M.F., A.A.N.B., K.J.O., D.A.R., K.J.S., F.P., A.S., A.L.G., R.S.K., J.R.C., and M.M.; Investigation, W.L.M., D.A.M.F., A.A.N.B., K.J.O., D.A.R., K.J.S., F.P., A.S., J.G.-G., M.V., and R.S.; Writing – Original Draft, W.L.M., D.A.M.F., A.L.G., R.S.K., J.R.C., and M.M.; Writing – Review & Editing, all authors; Funding Acquisition, D.A.M.F., A.L.G., R.S.K., J.R.C., and M.M.; Supervision, A.L.G., R.S.K., J.R.C., and M.M.

DECLARATION OF INTERESTS

Human BioMolecular Research Institute has filed a patent application on mexiletine analogs, in which J.R.C., K.J.O., and D.A.R. are co-inventors. M.M. serves on the scientific advisory board of Vala Sciences, which manufactures a high-content instrument used in these studies. A.L.G. serves on a scientific advisory board for cardiometabolic diseases at Amgen, Inc. The other authors declare no competing interests.

Received: April 25, 2020
Revised: June 27, 2020
Accepted: August 5, 2020
Published: September 14, 2020

REFERENCES

Al-Khatib, S.M., Stevenson, W.G., Ackerman, M.J., Bryant, W.J., Callans, D.J., Curtis, A.B., Deal, B.J., Dickfeld, T., Field, M.E., Fonarow, G.C., et al. (2018). 2017 AHA/ACC/HRS Guideline for Management of Patients With Ventricular Arrhythmias and the Prevention of Sudden Cardiac Death: A Report of the American College of Cardiology/American Heart Association Task Force on Clinical Practice Guidelines and the Heart Rhythm Society. Circulation *138*, e272–e391.

Bankston, J.R., Yue, M., Chung, W., Spyres, M., Pass, R.H., Silver, E., Sampson, K.J., and Kass, R.S. (2007). A novel and lethal *de novo* LQT-3 mutation in a newborn with distinct molecular pharmacology and therapeutic response. PLoS ONE *2*, e1258.

Belardinelli, L., Liu, G., Smith-Maxwell, C., Wang, W.Q., El-Bizri, N., Hirakawa, R., Karpinski, S., Li, C.H., Hu, L., Li, X.J., et al. (2013). A novel, potent, and selective inhibitor of cardiac late sodium current suppresses experimental arrhythmias. J. Pharmacol. Exp. Ther. *344*, 23–32.

Blinova, K., Dang, Q., Millard, D., Smith, G., Pierson, J., Guo, L., Brock, M., Lu, H.R., Kraushaar, U., Zeng, H., et al. (2018). International Multisite Study of Human-Induced Pluripotent Stem Cell-Derived Cardiomyocytes for Drug Proarrhythmic Potential Assessment. Cell Rep. *24*, 3582–3592.

Cerignoli, F., Charlot, D., Whittaker, R., Ingermanson, R., Gehalot, P., Savchenko, A., Gallacher, D.J., Towart, R., Price, J.H., McDonough, P.M., and Mercola, M. (2012). High throughput measurement of Ca^{2+} dynamics for drug risk assessment in human stem cell-derived cardiomyocytes by kinetic image cytometry. J. Pharmacol. Toxicol. Methods *66*, 246–256.

De Bellis, M., De Luca, A., Desaphy, J.F., Carbonara, R., Heiny, J.A., Kennedy, A., Carocci, A., Cavalluzzi, M.M., Lentini, G., Franchini, C., and Camerino, D.C. (2013). Combined modifications of mexiletine pharmacophores for new lead blockers of Na(v)1.4 channels. Biophys. J. *104*, 344–354.

De Luca, A., Natuzzi, F., Desaphy, J.F., Loni, G., Lentini, G., Franchini, C., Tortorella, V., and Camerino, D.C. (2000). Molecular determinants of mexiletine structure for potent and use-dependent block of skeletal muscle sodium channels. Mol. Pharmacol. *57*, 268–277.

De Luca, A., Talon, S., De Bellis, M., Desaphy, J.F., Franchini, C., Lentini, G., Catalano, A., Corbo, F., Tortorella, V., and Conte-Camerino, D. (2003). Inhibition of skeletal muscle sodium currents by mexiletine analogues: specific hydrophobic interactions rather than lipophilia per se account for drug therapeutic profile. Naunyn Schmiedebergs Arch. Pharmacol. *367*, 318–327.

Desaphy, J.F., De Luca, A., Tortorella, P., De Vito, D., George, A.L., Jr., and Conte Camerino, D. (2001). Gating of myotonic Na channel mutants defines the response to mexiletine and a potent derivative. Neurology *57*, 1849–1857.

Drawnel, F.M., Boccardo, S., Prummer, M., Delobel, F., Graff, A., Weber, M., Gérard, R., Badi, L., Kam-Thong, T., Bu, L., et al. (2014). Disease modeling and phenotypic drug screening for diabetic cardiomyopathy using human induced pluripotent stem cells. Cell Rep. *9*, 810–821.

Fabritz, L., Damke, D., Emmerich, M., Kaufmann, S.G., Theis, K., Blana, A., Fortmüller, L., Laakmann, S., Hermann, S., Aleynichenko, E., et al. (2010). Autonomic modulation and antiarrhythmic therapy in a model of long QT syndrome type 3. Cardiovasc. Res. *87*, 60–72.

Farre, C., and Fertig, N. (2012). HTS techniques for patch clamp-based ion channel screening—advances and economy. Expert Opin. Drug Discov. *7*, 515–524.

Feyen, D.A.M., McKeithan, W.L., Bruyneel, A.A.N., Spiering, S., Hörmann, L., Ulmer, B., Zhang, H., Briganti, F., Schweizer, M., Hegyi, B., et al. (2020). Metabolic Maturation Media Improve Physiological Function of Human iPSC-Derived Cardiomyocytes. Cell Rep. *32*, 107925.

Fiedler, L.R., Chapman, K., Xie, M., Maifoshie, E., Jenkins, M., Golforoush, P.A., Bellahcene, M., Noseda, M., Faust, D., Jarvis, A., et al. (2019). MAP4K4 Inhibition Promotes Survival of Human Stem Cell-Derived Cardiomyocytes and Reduces Infarct Size *In Vivo*. Cell Stem Cell *24*, 579–591.

Fridericia, L.S. (2003). The duration of systole in an electrocardiogram in normal humans and in patients with heart disease. 1920. Ann. Noninvasive Electrocardiol. *8*, 343–351.

Gualdani, R., Tadini-Buoninsegni, F., Roselli, M., Defrenza, I., Contino, M., Colabufo, N.A., and Lentini, G. (2015). Inhibition of hERG potassium channel by the antiarrhythmic agent mexiletine and its metabolite m-hydroxymexiletine. Pharmacol. Res. Perspect. *3*, e00160.

Hnatiuk, A., and Mercola, M. (2019). Stars in the Night Sky: iPSC-Cardiomyocytes Return the Patient Context to Drug Screening. Cell Stem Cell *24*, 506–507.

Horvath, B., and Bers, D.M. (2014). The late sodium current in heart failure: pathophysiology and clinical relevance. ESC Heart Fail. *1*, 26–40.

Hu, R.M., Tester, D.J., Li, R., Sun, T., Peterson, B.Z., Ackerman, M.J., Makielski, J.C., and Tan, B.H. (2018). Mexiletine rescues a mixed biophysical phenotype of the cardiac sodium channel arising from the SCN5A mutation, N406K, found in LQT3 patients. Channels (Austin) *12*, 176–186.

Koltun, D.O., Parkhill, E.Q., Elzein, E., Kobayashi, T., Notte, G.T., Kalla, R., Jiang, R.H., Li, X., Perry, T.D., Avila, B., et al. (2016). Discovery of triazolopyridine GS-458967, a late sodium current inhibitor (Late INai) of the cardiac NaV 1.5 channel with improved efficacy and potency relative to ranolazine. Bioorg. Med. Chem. Lett. *26*, 3202–3206.

Lu, H.R., Whittaker, R., Price, J.H., Vega, R., Pfeiffer, E.R., Cerignoli, F., Towart, R., and Gallacher, D.J. (2015). High Throughput Measurement of Ca++ Dynamics in Human Stem Cell-Derived Cardiomyocytes by Kinetic Image Cytometery: A Cardiac Risk Assessment Characterization Using a Large Panel of Cardioactive and Inactive Compounds. Toxicol. Sci. *148*, 503–516.

Maier, L.S., and Sossalla, S. (2013). The late Na current as a therapeutic target: where are we? J. Mol. Cell. Cardiol. *61*, 44–50.

Matsa, E., Ahrens, J.H., and Wu, J.C. (2016). Human Induced Pluripotent Stem Cells as a Platform for Personalized and Precision Cardiovascular Medicine. Physiol. Rev. *96*, 1093–1126.

Mazzanti, A., Maragna, R., Faragli, A., Monteforte, N., Bloise, R., Memmi, M., Novelli, V., Baiardi, P., Bagnardi, V., Etheridge, S.P., et al. (2016). Gene-Specific Therapy With Mexiletine Reduces Arrhythmic Events in Patients With Long QT Syndrome Type 3. J. Am. Coll. Cardiol. *67*, 1053–1058.

McKeithan, W.L., Savchenko, A., Yu, M.S., Cerignoli, F., Bruyneel, A.A.N., Price, J.H., Colas, A.R., Miller, E.W., Cashman, J.R., and Mercola, M. (2017). An Automated Platform for Assessment of Congenital and Drug-Induced Arrhythmia with hiPSC-Derived Cardiomyocytes. Front. Physiol. *8*, 766.

Miller, E.W., Lin, J.Y., Frady, E.P., Steinbach, P.A., Kristan, W.B., Jr., and Tsien, R.Y. (2012). Optically monitoring voltage in neurons by photo-induced electron transfer through molecular wires. Proc. Natl. Acad. Sci. USA *109*, 2114–2119.

Murphy, L.L., Moon-Grady, A.J., Cuneo, B.F., Wakai, R.T., Yu, S., Kunic, J.D., Benson, D.W., and George, A.L., Jr. (2012). Developmentally regulated SCN5A splice variant potentiates dysfunction of a novel mutation associated with severe fetal arrhythmia. Heart Rhythm *9*, 590–597.

Nuyens, D., Stengl, M., Dugarmaa, S., Rossenbacker, T., Compernolle, V., Rudy, Y., Smits, J.F., Flameng, W., Clancy, C.E., Moons, L., et al. (2001). Abrupt rate accelerations or premature beats cause life-threatening arrhythmias in mice with long-QT3 syndrome. Nat. Med. *7*, 1021–1027.

Priori, S.G., Blomström-Lundqvist, C., Mazzanti, A., Blom, N., Borggrefe, M., Camm, J., Elliott, P.M., Fitzsimons, D., Hatala, R., Hindricks, G., et al.; ESC Scientific Document Group (2015). 2015 ESC Guidelines for the management of patients with ventricular arrhythmias and the prevention of sudden cardiac death: The Task Force for the Management of Patients with Ventricular Arrhythmias and the Prevention of Sudden Cardiac Death of the European Society of Cardiology (ESC). Endorsed by: Association for European Paediatric and Congenital Cardiology (AEPC). Eur. Heart J. *36*, 2793–2867.

Roselli, M., Carocci, A., Budriesi, R., Micucci, M., Toma, M., Di Cesare Mannelli, L., Lovece, A., Catalano, A., Cavalluzzi, M.M., Bruno, C., et al. (2016). Synthesis, antiarrhythmic activity, and toxicological evaluation of mexiletine analogues. Eur. J. Med. Chem. *121*, 300–307.

Ruan, Y., Liu, N., Bloise, R., Napolitano, C., and Priori, S.G. (2007). Gating properties of SCN5A mutations and the response to mexiletine in long-QT syndrome type 3 patients. Circulation *116*, 1137–1144.

Ruan, Y., Denegri, M., Liu, N., Bachetti, T., Seregni, M., Morotti, S., Severi, S., Napolitano, C., and Priori, S.G. (2010). Trafficking defects and gating abnormalities of a novel SCN5A mutation question gene-specific therapy in long QT syndrome type 3. Circ. Res. *106*, 1374–1383.

Schroder, E.A., Burgess, D.E., Manning, C.L., Zhao, Y., Moss, A.J., Patwardhan, A., Elayi, C.S., Esser, K.A., and Delisle, B.P. (2014). Light phase-restricted feeding slows basal heart rate to exaggerate the type-3 long QT syndrome phenotype in mice. Am. J. Physiol. Heart Circ. Physiol. *307*, H1777–H1785.

Schwartz, P.J., Priori, S.G., Locati, E.H., Napolitano, C., Cantù, F., Towbin, J.A., Keating, M.T., Hammoude, H., Brown, A.M., Chen, L.S., and Colatsky, T.J. (1995). Long QT syndrome patients with mutations of the SCN5A and HERG genes have differential responses to Na+ channel blockade and to increases in heart rate. Implications for gene-specific therapy. Circulation *92*, 3381–3386.

Sharma, A., Burridge, P.W., McKeithan, W.L., Serrano, R., Shukla, P., Sayed, N., Churko, J.M., Kitani, T., Wu, H., Holmström, A., et al. (2017). High-throughput screening of tyrosine kinase inhibitor cardiotoxicity with human induced pluripotent stem cells. Sci. Transl. Med. *9*, eaaf2584.

Silver, E.S., Liberman, L., Chung, W.K., Spotnitz, H.M., Chen, J.M., Ackerman, M.J., Moir, C., Hordof, A.J., and Pass, R.H. (2009). Long QT syndrome due to a novel mutation in SCN5A: treatment with ICD placement at 1 month and left cardiac sympathetic denervation at 3 months of age. J. Interv. Card. Electrophysiol. *26*, 41–45.

Singh, S., Kerndt, C., and Zeltser, R. (2020). Mexiletine (StatPearls).

Spencer, C.I., Baba, S., Nakamura, K., Hua, E.A., Sears, M.A., Fu, C.C., Zhang, J., Balijepalli, S., Tomoda, K., Hayashi, Y., et al. (2014). Calcium transients closely reflect prolonged action potentials in iPSC models of inherited cardiac arrhythmia. Stem Cell Reports *3*, 269–281.

Stenson, P.D., Mort, M., Ball, E.V., Evans, K., Hayden, M., Heywood, S., Hussain, M., Phillips, A.D., and Cooper, D.N. (2017). The Human Gene Mutation Database: towards a comprehensive repository of inherited mutation data for medical research, genetic diagnosis and next-generation sequencing studies. Hum. Genet. *136*, 665–677.

Terrenoire, C., Wang, K., Tung, K.W., Chung, W.K., Pass, R.H., Lu, J.T., Jean, J.C., Omari, A., Sampson, K.J., Kotton, D.N., et al. (2013). Induced pluripotent stem cells used to reveal drug actions in a long QT syndrome family with complex genetics. J. Gen. Physiol. *141*, 61–72.

Tiscornia, G., Vivas, E.L., and Izpisúa Belmonte, J.C. (2011). Diseases in a dish: modeling human genetic disorders using induced pluripotent cells. Nat. Med. *17*, 1570–1576.

Zablocki, J.A., Elzein, E., Li, X., Koltun, D.O., Parkhill, E.Q., Kobayashi, T., Martinez, R., Corkey, B., Jiang, H., Perry, T., et al. (2016). Discovery of Dihydrobenzoxazepinone (GS-6615) Late Sodium Current Inhibitor (Late I_{Na}), a Phase II Agent with Demonstrated Preclinical Anti-Ischemic and Antiarrhythmic Properties. J. Med. Chem. *59*, 9005–9017.

Zhu, W., Mazzanti, A., Voelker, T.L., Hou, P., Moreno, J.D., Angsutararux, P., Naegle, K.M., Priori, S.G., and Silva, J.R. (2019). Predicting Patient Response to the Antiarrhythmic Mexiletine Based on Genetic Variation. Circ. Res. *124*, 539–552.

Please cite this article in press as: McKeithan et al., Reengineering an Antiarrhythmic Drug Using Patient hiPSC Cardiomyocytes to Improve Therapeutic Potential and Reduce Toxicity, Cell Stem Cell (2020), https://doi.org/10.1016/j.stem.2020.08.003

STAR★METHODS

KEY RESOURCES TABLE

REAGENT or RESOURCE	SOURCE	IDENTIFIER
Chemicals, Peptides, and Recombinant Proteins		
Y-27632 dihydrochloride	Tocris	1254
CHIR99021	Tocris	4423
Wnt-C59	Tocris	5148
VF2.1.Cl	(Miller et al., 2012)	N/A
Mexiletine hydrochloride	Toronto Research Chemical	M340800
Dofetilide	Tocris	3757
Tetrodotoxin citrate	Tocris	1069
GS-967	Medchem Express	HY-12593
Ranolazine dihydrochloride	Tocris	3118
Veratridine	Tocris	2918
ATX-II	Alomone Labs	STA-700
MexA1-A5	This study	**MexA1-MexA5**
Experimental Models: Cell Lines		
Human iPSC line (healthy donor)	SCVI Biobank	SCVI-273
Human iPSC line (healthy donor)	SCVI Biobank	SCVI-15S1
Human iPSC line (healthy donor)	SCVI Biobank	SCVI-113
Human iPSC line SCN5A F1473C	(McKeithan et al., 2017)	N/A
Human iPSC line SCN5A N406K	(Spencer et al., 2014)	N/A
MyCell Cardiomyocytes (SCN5A F1472C)	Cellular Dynamics International	Lot #: 1583.763.CM001
iCell Cardiomyocytes (healthy donor)	Cellular Dynamics International	Lot #s: 1097546, 1291715, 1093711, 1031999
CHO hERG-Duo Cell Line	Bsys	https://www.bsys.ch/
Software and Algorithms		
Cyteseer	Vala Sciences	http://www.valasciences.com/
GraphPad Prism 7	GraphPad Software	https://www.graphpad.com/scientific-software/prism/
PatchMaster	HEKA	http://www.heka.com/
PatchLiner Data acquisition	Nanion	https://www.nanion.de/en/
Origin 7.0	OriginLab	https://www.originlab.com/
IgorPro	WaveMetrics	https://www.wavemetrics.com/
MATLAB	Mathworks	https://www.mathworks.com/
PatchController384 V.1.3.0	Nanion	https://www.nanion.de/en/
DataController384 V1.2.1	Nanion	https://www.nanion.de/en/
pClamp 10.2	Molecular Devices	https://www.moleculardevices.com/
ChemDraw Ultra version 11	PerkinElmer	https://www.perkinelmer.com/

RESOURCE AVAILABILITY

Lead Contact

Further information and requests for resources and reagents should be directed to and will be fulfilled by the Lead Contact, Mark Mercola (mmercola@stanford.edu).

Materials availability

All unique reagents generated in this study are available from the Lead Contact with a completed Materials Transfer Agreement.

Data and Code Availability

The published article includes all datasets generated or analyzed during this study. This study did not generate code.

EXPERIMENTAL MODEL AND SUBJECT DETAILS

iCell Cardiomyocyte Culture (corresponds to Figure 2)

MyCell Cardiomyocytes (LQT3) referred to as (SCN5A F1473C) and iCell Cardiomyocytes (healthy donor) referred to as (HD.CDI) (Cellular Dynamics International, Wisconsin, USA) were used for optical assessment of AP kinetics and whole cell patch clamp recording (Figure 2). The LQT3 cells were from a male. The HD.CDI iCell Cardiomyocytes were from a female. Purity of MyCell Cardiomyocytes was $\geq$ 97% hiPSC-CMs and iCell Cardiomyocytes was $\geq$ 99% hiPSC-CMs (as per CDI data sheets). Cryopreserved vials were thawed according to the manufacturer's specifications. The vial was transferred to a 37°C water bath for 4min. Once completely thawed, the contents were slowly transferred to a 50 mL conical vial and diluted dropwise in iCell Cardiomyocyte Plating Media (iCCPM) to a concentration of 2.5 × 10^5 cells/mL. hiPSC-CMs were transferred into 384 well plates pre-coated (Greiner Bio-One) with 0.1% (w/v) gelatin (Stem Cell Technologies). The plates were then placed in a 37°C incubator with 5% CO_2. After 24 hours, the media was exchanged with iCell Cardiomyocyte Maintenance Media (iCCMM), supplemented with 5mM D-glucose. This process was repeated two additional times, ultimately yielding a final volume of 100 μL/well. Media was exchanged every other day for 14 days prior to imaging by removing 50 μL of media and adding 50 μL of fresh iCCMM (supplemented with 5 mM D-glucose).

Differentiation of hiPSCs to cardiomyocytes (corresponds to Figure 4)

Healthy donor cells (HD.113, HD.15S1, HD.273) were obtained from the Stanford CVI Biobank and originally derived under a Stanford University IRB approved protocol. Healthy donor [HD.113 (male), HD.15S1 (male), HD.273 (female)] and LQT3 [SCN5A F1473C (male) and SCN5A N406K (female)] hiPSCs were differentiated and used for tertiary assays shown in Figure 4. Briefly, hiPSCs were dissociated using 0.5 mM EDTA (ThermoFisher Scientific, Waltham, MA, USA) in PBS without $CaCl_2$ or $MgCl_2$ (Corning, New York, USA) for 7 minutes at room temperature. The dissociated hiPSCs were plated in growth factor reduced matrigel-coated dishes in E8 culture media (ThermoFisher Scientific, Waltham, MA, USA) supplemented with 1 μM Y-27632 (Tocris, Bristol, UK). After 24 hours, the media was replaced with E8 without Y-27632 and was replenished daily for 3-5 days until the cells reached $\geq$ 90% confluence to begin differentiation. Cardiomyocytes were differentiated by methods previously described (Feyen et al., 2020). Briefly, hiPSCs were treated with 4-8 μM CHIR99021 (Tocris, Bristol, UK), depending on the hiPSC line used for differentiation, for 3 days in RPMI 1640 supplemented with B27 without insulin (RPMI/B27-). Subsequently, the cells were treated with 2 μM Wnt inhibitor C59 (Tocris, Bristol, UK) in RPMI/B27- for another 2 days. Between 5–11 days of differentiation, RPMI/B27- media was used and changed every other day until beating cells were observed when the media was switched to RPMI 1640 supplemented with B27 with insulin (RPMI/B27+). To improve the CM purity, cells were cultured in RPMI/B27+ without glucose, but supplemented with 5 mM sodium L-lactate for 3 days. On day 14, the hiPSC-CMs were dissociated with TrypLE 10x for 10 minutes (or until the cells lifted from the plate) and seeded in 6-well Matrigel coated plates at a density of 3x10^6 per well in RPMI/B27+ containing 10% Knockout Serum Replacement (KOSR) and ROCK inhibitor Y-27632 (Tocris, Bristol, UK). hiPSC-CMs were cultured in RPMI/B27+ with glucose for 3-5 days prior to switching to 3 mL of maturation media in each well of a 6 well plate (Feyen et al., 2020). Maturation media was composed as follows: DMEM without glucose (Thermo Fisher Scientific, 11966025) supplemented with 3 mM glucose (Sigma Aldrich, G7021), 10 mM L-lactate (Sigma Aldrich, 71718), 5 μg/ml Vitamin B12 (Sigma Aldrich, V6629), 0.82 μM Biotin (Sigma Aldrich, B4639), 5 mM Creatine monohydrate (Sigma Aldrich, C3630), 2 mM Taurine (Sigma Aldrich, T0625), 2 mM L-carnitine (Sigma Aldrich, C0283), 0.5 mM Ascorbic acid (Sigma Aldrich, A8960), 1x NEAA (Thermo Fisher Scientific, 11140), 0.5% (w/v) Albumax (Thermo Fisher Scientific, 11020021), 1x B27 and 1% KOSR (Thermo Fisher Scientific, 10828028). Cells were kept in maturation media culture for 3-4 weeks with media changes occurring every 4 days. For the optical voltage assay, cells were dissociated similarly to day 14 and replated in maturation media with 10% KOSR and Y-27632 and plated onto Matrigel-coated 384-well tissue culture plates (Greiner Bio-One, Kremsmünster, Austria) at a density of 20,000 cells/well.

METHOD DETAILS

High throughput optical action potential recording

All dye loading and compound administration methods were described and validated in detail in McKeithan et al. (2017). 384 well plates containing hiPSC-CMs were placed on a 37°C heated surface for all manipulations to prevent temperature fluctuation. Each well was washed to remove the tissue culture media and replaced with Tyrode's solution. VF2.1.Cl (Miller et al., 2012) loading solution was prepared as described in McKeithan et al. (2017). Each plate was incubated at 37°C in a 5% CO_2 incubator for 50 min. After incubation with VF2.1.Cl solution, each well was washed with Tyrode's solution. Each test compound was loaded and incubated for 5 minutes prior to imaging. Time series images were acquired at 100Hz using an IC200 KIC instrument (Vala Sciences, California, USA) with excitation wavelength of 485/20 nm and emission filter 525/30 nm using a 0.75 NA 20x Nikon Apo VC objective. Image analysis was conducted using Cyteseer (Vala Sciences, California, USA) as previously described (Cerignoli et al., 2012; Lu et al., 2015; McKeithan et al., 2017). The output images from the IC200 KIC were loaded into Cyteseer and a whole well cardiac time series algorithm was executed on the image files. Physiological parameters (beat rate, normalized area under the peak trace (normalized peak integral), and APD_{25}, APD_{50}, APD_{75} and APD_{90}) were automatically calculated for each time series. EADs were

Please cite this article in press as: McKeithan et al., Reengineering an Antiarrhythmic Drug Using Patient hiPSC Cardiomyocytes to Improve Therapeutic Potential and Reduce Toxicity, Cell Stem Cell (2020), https://doi.org/10.1016/j.stem.2020.08.003

quantified automatically by identifying peaks following a local minimum above a user defined threshold above the diastolic interval minimum. Data tables were analyzed with Microsoft Excel and dose responses and heatmaps were generated with GraphPad Prism 7 software.

Ion channel modulators were purchased: Mexiletine (Toronto Research Chemical, Toronto, Canada), dofetilide (Tocris, Bristol, UK), tetrodotoxin (Tocris Bristol, UK), GS-967 (Medchem Express, Monmouth Junction, NJ, USA), ranolazine (Tocris, Bristol, UK), veratridine (Tocris, Bristol, UK) and ATX-II (Alomone Labs, Jerusalem, Israel).

Automated planar patch clamp

Whole cell planar patch clamp recordings were used to directly study the effects of test compounds on ion channel currents: I_{NaP}, I_{NaL}, and I_{Kr} (hERG) channels (Farre and Fertig, 2012). In all experiments the number of cells studied (n) for each drug concentration cited was indicated.

For dose response studies (Figures 2E–2I), at least 6 increasing concentrations were included. For Na^+ channel experiments, we used a stable HEK cell line expressing a long QT mutant, F1473C (Bankston et al., 2007), and for I_{Kr} we used a commercially available CHO stable cell line, hERG Duo (Bsys, Switzerland). Normalized blocking ratio data, for each of I_{Kr}, I_{NaP} and I_{NaL}, were fitted by a 4-parameter logistic fit. The following solutions were used in these experiments: Internal solution for K^+ channel experiments: 50 mM KCl, 10 mM NaCl, 60 mM K-Fluoride, 20 mM EGTA, and 10 mM HEPES/KOH, pH 7.2. Internal solution for Na^+ channel experiments: 50 mM CsCl, 10 mM NaCl, 60 mM Cs-Fluoride, 20 mM EGTA, 10 mM HEPES/CsOH, pH 7.2 External solutions for K^+ and Na^+ channel experiments: 140 mM NaCl, 4 mM KCl, 1mM $MgCl_2$, 5 mM D-glucose monohydrate, and10 mM HEPES/NaOH pH 7.4. Control experiments contained 0.01% DMSO as did all drug containing solutions. Reagents were obtained from Sigma-Aldrich (St Louis, MO, USA). Patch clamp data were acquired with PatchMaster (HEKA, Germany) and PatchLiner Data acquisition (Nanion, Munich, Germany) and analyzed with Origin 7.0 (OriginLab, Northampton, MA, USA) and IgorPro (WaveMetrics, Portland, OR, USA) and MATLAB (Mathworks, Natick, MA, USA). Data were shown as mean ± SEM. Statistical data analyses was assessed with Student's t test. Differences at $p < 0.05$ were considered as statistically significant.

For the study of LQT3-causing SCN5A mutations, plasmids encoding WT and LQT3-mutations were transiently transfected into HEK293T cells by electroporation using the Maxcyte STX system (MaxCyte Inc., Gaithersburg, MD, USA). HEK293T cells were grown to 70%–80% confluency and then harvested using 5% trypsin, then a 500 μl aliquot of cell suspension was used to determine cell number and viability on an automated cell counter (ViCell, Beckman Coulter, Brea, CA, USA). Remaining cells were collected by gentle centrifugation (160 × g, 4 minutes), then the cell pellet was washed with 3 mL electroporation buffer (EBR100, MaxCyte Inc., Gaithersburg, MD, USA) and re-suspended in electroporation buffer at a density of 10^8 viable cells/ml. For each electroporation, plasmids encoding WT or LQT3-causing SCN5A mutations (40 μg) were added to 100 μl cell suspension (10^8 cells/ml). The DNA-cell suspension mix was then transferred to an OC-100 processing assembly (MaxCyte Inc., Gaithersburg, MD, USA) and electroporated using the optimization-5 preset protocol. Immediately after electroporation, 10 μl of DNase I (Sigma-Aldrich, St. Louis, MO, USA) was added to the DNA-cell suspension and the entire mixture was transferred to a 60 mm tissue culture dish and incubated for 30 min at 37°C in 5% CO_2. Following incubation, cells were gently re-suspended in culture media, transferred to a T75 tissue culture flask and grown for 48 hours at 37°C in 5% CO_2. Following incubation, cells were harvested, counted and re-suspended in external solution at 180,000 cells/ml. Cells were allowed to recover for at least 30 min at 15°C while shaking on a rotating platform. Following equilibration, 10 μl of cell suspension was added to each well of a 384-well, single-hole, low resistance (2 MΩ) 'chip' (Nanion Technologies, München, Germany). Whole-cell currents were recorded at room temperature in the whole-cell configuration. The external solution contained (in mM) the following: NaCl 140, KCl 4, $CaCl_2$ 2, $MgCl_2$ 1, HEPES 10, glucose 5, pH = 7.4). The internal solution contained (in mM) the following: CsF 110, CsCl 10, NaCl 10, HEPES 10, EGTA 20, pH = 7.2. Automated patch clamp recording was conducted using a Syncropatch 768PE (Nanion Technologies, Munich, Germany) using single hole low resistance 384-well patch plates. Pulse generation and data collection were done with PatchController384 V.1.3.0 and DataController384 V1.2.1 (Nanion Technologies). Whole-cell currents were filtered at 3 kHz and acquired at 10 kHz. The access resistance and apparent membrane capacitance were estimated using built-in protocols. Series resistance was compensated 95% and leak and capacitance artifacts were subtracted out using the P/4 method. Cells were excluded from analysis if the maximum peak current was less than 300 pA. Test compounds were diluted in the external solution and prepared in a separate 24 wells plate. DMSO concentration was the same for each compound.

hiPSC-CM electrophysiology

Sodium currents were recorded from single hiPSC-CMs using the whole-cell patch-clamp technique. 5mm coverslips were coated with a 0.1% gelatin solution. hiPSC-CMs were plated and cultured for at least 2 weeks prior to recording. Each coverslip was transferred to a recording chamber (RC-25-F, Warner Instruments, Hamden, CT) perfused with Tyrode's solution that was mounted on the stage of an inverted Olympus microscope. Patch pipettes were pulled glass capillaries (CORNING 7740, 1.65mm) with a P-2000 laser pipette puller (Sutter Instruments, Novato, CA, USA). Pipettes had electrode tip resistance of 1.5 MΩ to 5.5 MΩ and access resistance of < 8MΩ. In some voltage recordings, series resistance and cell capacitance were compensated 30 to 60%. The intracellular solution consisted of 120 mM CsCl, 20 mM tetraethylammonium chloride (TEA-Cl), 10 mM HEPES, 2.25 mM EGTA, 1 mM $CaCl_2$, 2 mM $MgCl_2$, pH 7.4. All recordings were conducted at room temperature. Current response traces were acquired using the Axon 200B amplifier and were digitally sampled at 10 kHz using Digidata 1322A digitizer hardware and pClamp 10.2 software (Molecular Devices, San Jose, CA, USA). Current responses were filtered with an 8-pole Bessel analog low-pass filter at 1-2 kHz cutoff frequency. Current

amplitude at the end of the depolarizing step was corrected by the leak current and the corrected current amplitude was averaged for n = 10 cells. After the leak-correction, the average value of the recorded current amplitude was computed over the last 50 ms of the 150 ms depolarizing pulse of each 250 ms sweep. The resulting value was averaged over 3 consecutive sweeps.

Chemistry

Chemical names were generated with ChemDraw Ultra version 11 (PerkinElmer, Waltham, MA, USA). Experiments were carried out under inert atmosphere when oxygen- or moisture-sensitive reagents or intermediates were employed. Commercial solvents and reagents were used without further purification. Mexiletine was purchased from Toronto Research Chemicals (Ontario, Canada). 2-(2,6-dimethylphenoxy)-1-phenylethan-1-amine (phenyl mexiletine, **MexA1**) was purchased from Millipore Sigma (Burlington, MA, USA).

Microwave reactions were conducted using a Biotage Initiator microwave synthesizer (Biotage, Uppsala, Sweden). Reaction products were purified, when necessary, using an Isco Combiflash R_f flash chromatography system (Teledyne-Isco, Lincoln, NE, USA) with the solvent systems indicated. Nuclear magnetic resonance (NMR) data were recorded on a Varian Mercury 300 MHz Spectrometer (Agilent, Santa Clara, CA, USA) or with a Bruker 500 MHz instrument at NuMega Resonance Laboratories (San Diego, CA, USA) using $CDCl_3$ as a solvent except where indicated. Chemical shifts for nuclear magnetic resonance (NMR) data were expressed in parts per million (ppm, δ) referenced to residual peaks from the deuterated solvents. Mass spectrometry (MS) data was reported from liquid chromatography-mass spectrometry (LCMS) instrumentation. Electrospray ionization (ESI) mass spectral data was obtained using an Agilent 1100 LC/MS (Agilent, Santa Clara, CA, USA). Final test compounds had a purity greater than 95% based on LCMS analysis using UV-Vis detection at 275 nM and 220 nM.

Illustration of methods for the synthesis of compounds MexA2-5

1-Phenyl-2-(o-tolyloxy)ethan-1-amine (MexA2)

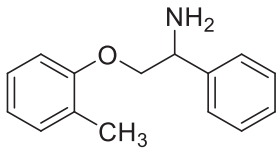

Step 1: 1-phenyl-2-(o-tolyloxy)ethan-1-one

To a solution of α-bromoacetophenone (1.0 g, 5.0 mmol) and 2-methylphenyl (0.65 g, 6.0 mmol) in 5 mL of DMF added potassium carbonate (0.83 g, 6.0 mmol). The mixture was stirred at 21°C for 16 h and then diluted with water. The product was extracted with ether. The organic phase was washed (1M sodium hydroxide, water, brine), dried (magnesium sulfate) and subjected to chromatography on silica gel using a gradient of ethyl acetate in hexanes to afford 0.61 g (45%) of the product as an off white solid.

ESI/MS: calculated $C_{15}H_{14}O_2$ *m/z* = 226.1, found *m/z* = 227.0 $[M+H]^+$.

^{1}H NMR ($CDCl_3$): 2.30 (s, 3H), 5.26 (s, 2H), 6.75 (d, J = 8.0 Hz, 1H), 6.89 (t, J = 7.5 Hz, 1H), 7.09 – 7.17 (m, 2H), 7.46 – 7.51 (m, 2H), 7.58 – 7.64 (m, 1H), 7.99 – 8.02 (m, 2H).

Step 2: 1-phenyl-2-(o-trolley)ethanone O-benzyl oxime

To 0.2 g (0.9 mmol) of 1-phenyl-2-(o-tolyloxy)ethan-1-one in 5 mL of ethanol was added pyridine (0.35 mL, 4.4 mmol) and O-benzylhydroxylamine (0.51 mL, 4.4 mmol). The mixture was stirred at 40°C for 16 h, treated with additional pyridine (0.17 mL, 2.2 mmol) and O-benzylhydroxylamine (0.25 mL, 2.2 mmol) and stirred at 55°C for additional 16 h. The volatiles were removed under reduced pressure and the residue was partitioned between aqueous 1M hydrochloric acid and ether. The organic phase was washed (water, brine) and dried over magnesium sulfate. The oxime was purified by chromatography on silica gel using a mixture of ether and hexanes to afford the product as a mixture of E/Z isomers (64 mg, 21% yield).

ESI/MS: calculated $C_{22}H_{21}NO_2$ *m/z* = 331.2, found *m/z* = 332.0 $[M+H]^+$.

^{1}H NMR ($CDCl_3$): 2.03 (s,3H), 5.25 (s, 2H), 5.29 (s, 2H), 6.80 – 6.89 (m, 2H), 7.03 – 7.09 (m, 2H), 7.31 – 7.45 (m, 9H), 7.63 – 7.66 (m, 1H).

1-Phenyl-2-(o-tolyloxy)ethan-1-amine (MexA2)

A solution of 30 mg (0.09 mmol) of the above oxime in 0.4 mL of THF was treated with 0.4 mL of 1M borane-THF (0.4 mmol) and stirred at 21°C for 16 h. The mixture was treated with 1M aqueous hydrochloric acid and extracted with ether. The combined organic phases were dried over sodium sulfate. The crude product was purified by preparative thin layer chromatography and the product was treated with an excess of hydrogen chloride in ether. The precipitated solid was filtered, rinsed with ether and vacuum dried to afford the product as a hydrochloride salt (16.4 mg, 68% yield).

ESI/MS: calculated $C_{15}H_{17}NO$ *m/z* = 227.1, found *m/z* = 228.0 $[M+H]^+$.

^{1}H NMR ($CDCl_3$): 2.24 (s, 3H), 2.88 (bs, 2H), 3.98 – 4.05 (m, 1H), 4.13 (dd, J = 4.1 Hz and 9.1 Hz, 1H), 4.45 – 4.49 (m, 1H), 6.75 – 6.78 (m, 1H), 6.83 – 6.88 (m, 1H), 7.08 – 7.13 (m, 2H), 7.29 – 7.37 (m, 4H), 7.44 – 7.47 (m, 1H).

The following compounds were generated by the sequence described above with appropriate modifications:

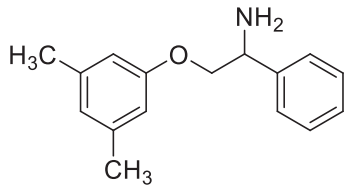

2-(3,5-Dimethylphenoxy)-1-phenylethan-1-amine (MexA3)

ESI/MS: calculated *m/z* for $C_{16}H_{19}NO$: 241.1 Found *m/z*: 242.1 $[M+H]^+$.

1H NMR (300 MHz, Methanol-d4) δ 7.42 – 7.58 (m, 4H), 7.42 – 7.58 (m, 4H), 6.64 (s, 3H), 4.73 (dd, J = 4.1, 8.4 Hz, 1H), 4.18 – 4.38 (m, 2H), 2.27 (d, J = 0.7 Hz, 6H).

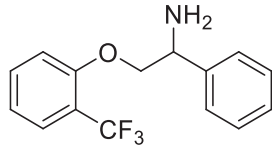

1-Phenyl-2-(2-(trifluoromethyl)phenoxy)ethan-1-amine (MexA4)

ESI/MS: calculated $C_{15}H_{14}F_3NO$ *m/z* = 281.1, found *m/z* = 282.0 $[M+H]^+$.

1H NMR (CDCl3): 2.38 (bs, 2H), 4.02 – 4.11 (m, 1H), 4.19 – 4.27 (m, 1H), 4.48 – 4.58 (m, 1H), 6.91 – 6.94 (m, 1H), 6.98 – 7.03 (m, 1H), 7.29 – 7.42 (m, 4H), 7.44 – 7.49 (m, 2H), 7.54 – 7.58 (m, 1H).

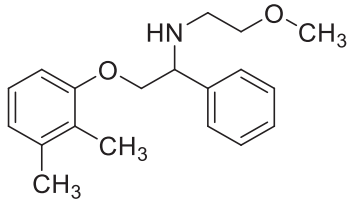

2-(2,3-dimethylphenoxy)-N-(2-methoxyethyl)-1-phenylethan-1-amine (MexA5)

This compound was synthesized in two steps from the precursor 2-(2,3-dimethylphenoxy)-1-phenylethan-1-amine, which in turn was generated by the method described above.

Properties for precursor precursor 2-(2,3-dimethylphenoxy)-1-phenylethan-1-amine:

ESI/MS: calculated *m/z* for $C_{16}H_{19}NO$: 241.1 Found *m/z*: 242.0 $[M+H]^+$.

^{1}H NMR (300 MHz, $CDCl_3$) δ 7.47 (d, *J* = 7.43 Hz, 1H), 7.28 - 7.43 (m, 4H), 7.02 (t, *J* = 7.84 Hz, 1H), 6.79 (d, *J* = 7.70 Hz, 1H), 6.68 (d, *J* = 7.98 Hz, 1H), 4.47 (dd, *J* = 3.85, 8.25 Hz, 1H), 4.10 (dd, *J* = 3.85, 9.08 Hz, 1H), 3.87 - 4.04 (m, 1H), 2.23 - 2.35 (m, 3H), 2.11 - 2.22 (m, 3H)

Step 1: N-(2-(2,3-dimethylphenoxy)-1-phenylethyl)-2-methoxyacetamide.

To a solution of 2-methoxyacetic acid (0.068 mL, 0.89 mmol) and trimethylamine (0.126 mL, 0.9 mmol) in dichloromethane (1 mL) added 400 mg (0.9 mmol) of (Benzotriazol-1-yloxy)tris(dimethylamino)phosphonium hexafluorophosphate (BOP). After 5 min a solution of 198 mg (0.82 mmol) of 2-(2,3-dimethylphenoxy)-1-phenylethan-1-amine was added. After stirring overnight at room temperature, the mixture was diluted with ethyl acetate. The organic phase was washed (water, saturated aqueous sodium bicarbonate, water and brine) and dried over magnesium sulfate. The crude product was purified on silica gel using a methanol:dichloromethane gradient. 156 mg (61%) of the target compound was obtained.

R_f = 0.7 (19:1 dichloromethane:methanol)

^{1}H NMR (300 MHz, $CDCl_3$) δ 7.22 - 7.49 (m, 5H), 7.04 (t, *J* = 7.98 Hz, 1H), 6.80 (d, *J* = 7.70 Hz, 1H), 6.68 (d, *J* = 8.25 Hz, 1H), 5.39 - 5.59 (m, 1H), 4.18 - 4.39 (m, 2H), 3.97 (s, 2H), 3.39 - 3.51 (m, 3H), 2.28 (s, 3H), 2.10 - 2.18 (m, 3H)

Step 2: 2-(2,3-dimethylphenoxy)-N-(2-methoxyethyl)-1-phenylethan-1-amine.

A solution of 156 mg (0.5 mmol) of N-(2-(2,3-dimethylphenoxy)-1-phenylethyl)-2-methoxyacetamide in 3.0 mL of THF was added dropwise at room temperature to a 1 M solution of lithium aluminum hydride in THF (2.4 mL, 2.4 mmol). The mixture was then heated at 75°C overnight. The mixture was cooled in an ice/brine bath and treated with water (0.087 mL) followed by 1M aq NaOH (0.087 mL). The precipitate was removed by filtration and rinsed with ethyl acetate. The filtrate was dried over magnesium sulfate, concentrated and purified by chromatography using a methanol dichloromethane gradient to afford the amine free base as a colorless oil.

^{1}H NMR (300 MHz, $CDCl_3$) δ 7.18 - 7.54 (m, 5H), 6.91 - 7.07 (m, 1H), 6.77 (d, *J* = 7.43 Hz, 1H), 6.65 (d, *J* = 7.98 Hz, 1H), 4.11 - 4.22 (m, 1H), 3.92 - 4.11 (m, 2H), 3.43 - 3.60 (m, 2H), 3.38 (s, 3H), 2.59 - 2.87 (m,2H), 2.29 (s, 3H), 2.18 (s, 3H).

Please cite this article in press as: McKeithan et al., Reengineering an Antiarrhythmic Drug Using Patient hiPSC Cardiomyocytes to Improve Therapeutic Potential and Reduce Toxicity, Cell Stem Cell (2020), https://doi.org/10.1016/j.stem.2020.08.003

The oil was dissolved in ether (9 mL) and treated with 4M HCl in dioxane (0.5 mL, 2.0 mmol). Hexanes and toluene were added and the mixture was evaporated under reduced pressure. The residue was treated with hexane:ether and the solid obtained was filtered, rinsed with hexanes and vacuum dried. 56 mg (33%) of the hydrochloride salt was obtained.

ESI/MS: calculated *m/z* for $C_{16}H_{25}NO_2$: 299.1 Found *m/z*: 300.1 $[M+H]^+$.

^{1}H NMR (300 MHz, DMSO-d_6) δ 9.89 – 9.27 (br.d., 2H), 7.64 (br. s., 1H), 7.16 - 7.60 (m, 3H), 7.02 (br. s., 1H), 6.77 (br. s., 1H), 4.77 (br. s., 1H), 4.51 (br. s., 1H), 4.34 (br. s., 1H), 3.74 – 3.46 (m., 2H), 3.33 - 3.43 (m, 2H), 3.30 (s, 3H), 2.18 (s, 3H), 1.99 (s, 3H)

QUANTIFICATION AND STATISTICAL ANALYSIS

Data are presented as mean ± standard error of the mean (SEM) as indicated. Statistical analysis was conducted using GraphPad Prism 7 (GraphPad Software, Inc., San Diego, CA). Concentration-dependent IC_{50} curves were fitted using a log(inhibitor) versus response – variable slope (four parameters). Significance was calculated using the two-tailed unpaired Student's t tests. Data that were not normally distributed were tested using the Mann–Whitney–Wilcoxon test. One-way ANOVA with Dunnett's method was used for multiple comparisons. P value < 0.05 was considered statistically significant.

Cell Stem Cell, Volume *27*

Supplemental Information

Reengineering an Antiarrhythmic Drug Using Patient hiPSC Cardiomyocytes to Improve Therapeutic Potential and Reduce Toxicity

Wesley L. McKeithan, Dries A.M. Feyen, Arne A.N. Bruyneel, Karl J. Okolotowicz, Daniel A. Ryan, Kevin J. Sampson, Franck Potet, Alex Savchenko, Jorge Gómez-Galeno, Michelle Vu, Ricardo Serrano, Alfred L. George Jr., Robert S. Kass, John R. Cashman, and Mark Mercola

Supplementary Information

Figure S1

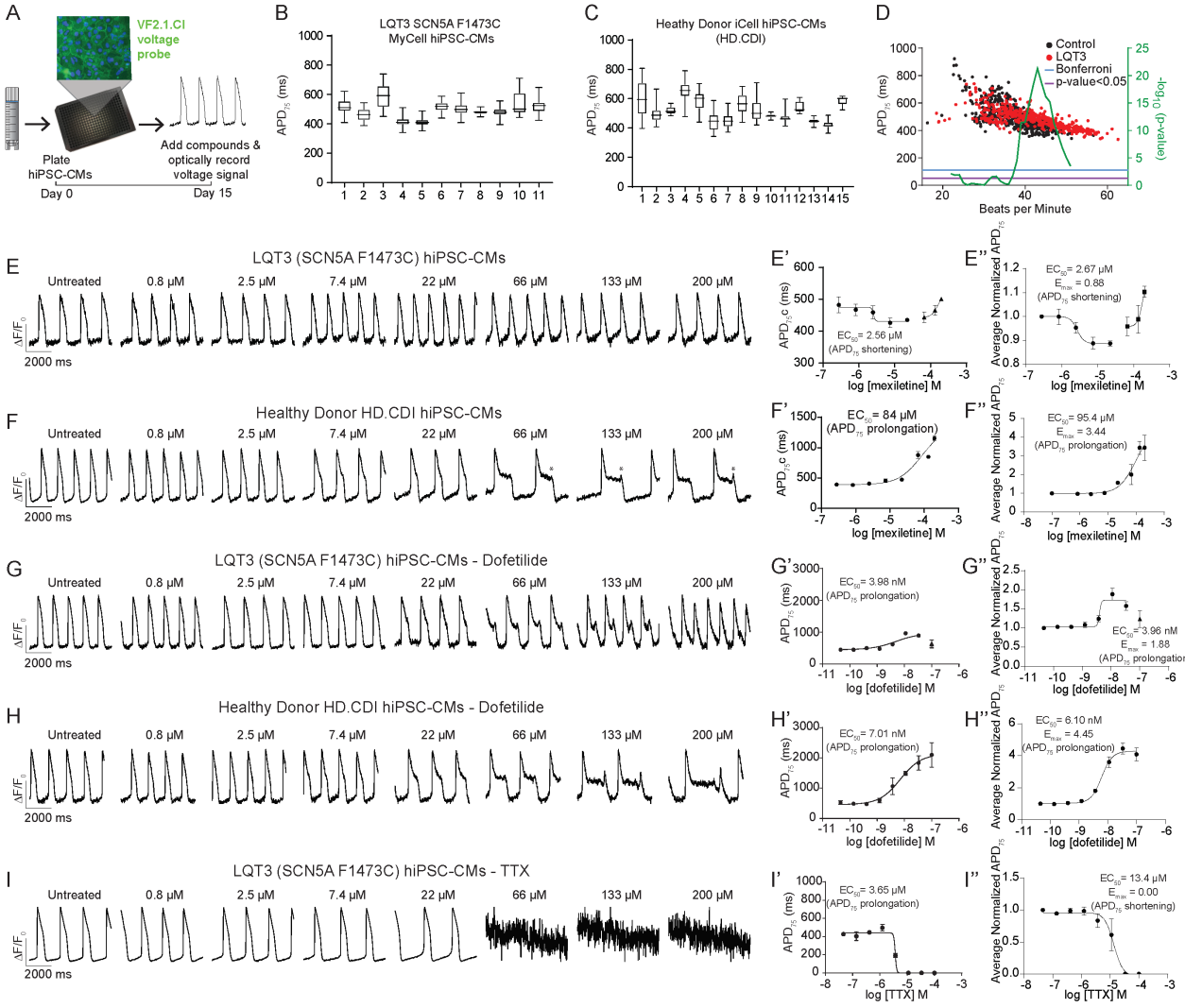

Figure S1. Assay development. Related to Figure 1.

A) Schematic for CDI hiPSC-CM workflow. CDI iCell or MyCell hiPSC-CMs were cultured for 14 days prior to loading with VF2.1.Cl and addition of mexiletine analogues.

B) APD_{75} of all healthy donor CDI iCell hiPSC-CMs (HD.CDI) thaws used for screening. Figure updated from (McKeithan et al., 2017)

C) APD_{75} of all LQT3 F1473C CDI MyCell hiPSC-CMs (SCN5A F1473C) thaws used for screening. Figure updated from (McKeithan et al., 2017)

D) Plot of average APD_{75} vs. spontaneous beat rate (BPM) from individual LQT3 and healthy donor (HD.CDI iCell) cardiomyocyte wells. Mann-Whitney test using a sliding window (center value ± 3) (green) with Mann Whitney p-value < 0.05 (purple) and Bonferroni corrected p-value (blue). Note that APD_{75} values show prolongation relative to healthy donor values between about 38-50 BPM. Panel **D** was reproduced with permission from (McKeithan et al., 2017).

E) Representative dose series of optical voltage traces (6 s, 100 fps) showing AP shortening of LQT3 patient hiPSC-CMs (SCN5A F1473) used in the primary screening in response to mexiletine (**E**). Dose response (**E'**, error bars ± sem, n=4) showed shortening of APD_{75}. Graph indicates effect on AP duration at the point of 75% decay from peak height (APD_{75}). The dose responsiveness is highly reproducible across experiments (**E"**, error bars ± sem, n=5 independent experiments as in **E'**). Panel **E"** was reproduced with permission from (McKeithan et al., 2017).

F) As in (**E**) except for healthy donor-derived hiPSC-CMs (hiPSC line HD.CDI) used in primary screening. ***** indicates incidence of proarrhythmic response.

G) LQT3 patient hiPSC-CMs as in (**E**) except for treatment with the K^+ channel blocker, dofetilide, as a positive control for APD prolongation and induction of early after depolarizations (EADs).

H) HD.CDI hiPSC-CMs treated with dofetilide as in (**G**).

I) Dose response of the Na^+ channel blocker Tetrodotoxin (TTX) to establish that the AP depends on Na^+ channel function in hiPSC-CMs generated from the LQT3 SCN5A F1473C donor.

Error bars (**E'-I'**) indicate mean ± SEM, n=4 replicates. Error bars (**E''-I''**) indicate mean ± SEM, n=5 independent experiments.

Figure S2

Effect of mexiletine and phenyl mexiletine analogues (MexA2-5) on AP kinetics (optically assessed) and Na+ and hERG currents (automated planar patch clamp). Related to Figure 2.

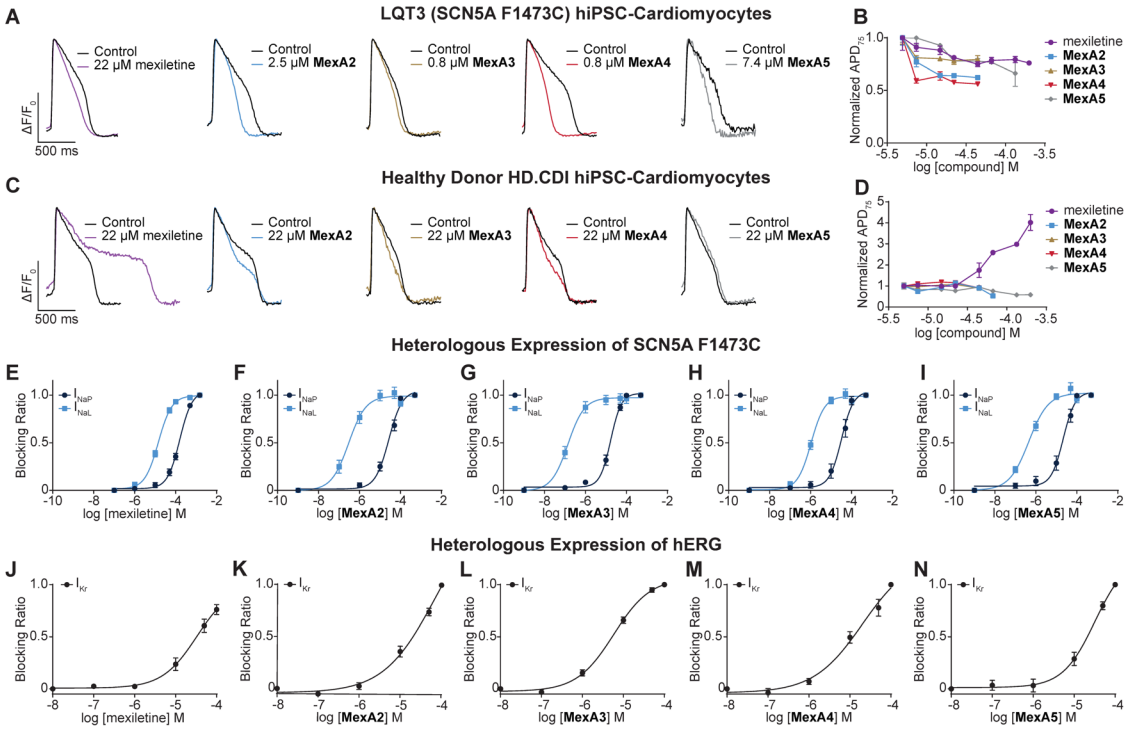

Effect of mexiletine and MexA2-5 analogues on different LQT3-causing SCN5A mutations (individual data points for Figure 3B,C). Related to Figure 3.

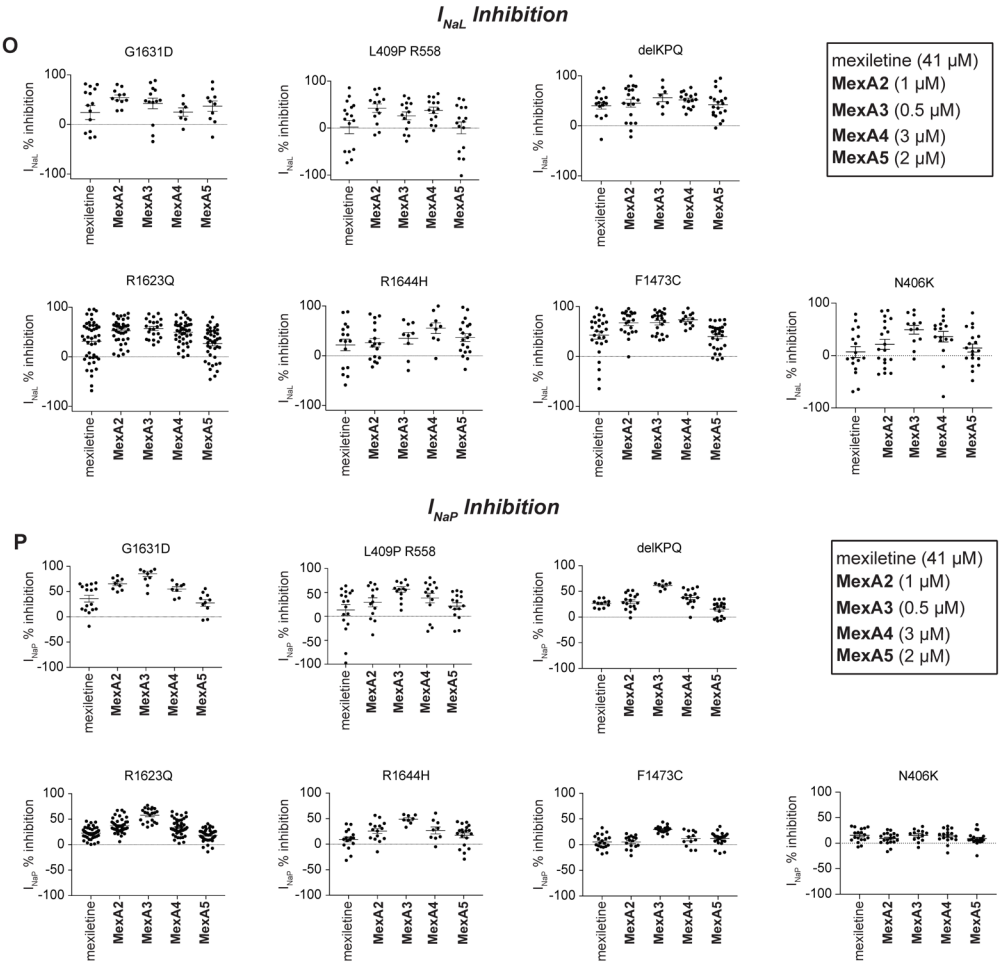

Figure S2. Effect of mexiletine and MexA2-5 analogues on AP kinetics (optically assessed), I_{Na} and I_{Kr} inhibition (automated planar patch clamp), and I_{Na} inhibition across a panel LQT3 causing SCN5A variants. Related to Figure 2 and Figure 3.

A,C) Representative optical AP recordings of action potentials from a single dose (22 μM) from a dose-escalation of mexiletine and **MexA2-5** analogues in hiPSC-CMs generated from LQT3 SCN5A F1473C (**A**) and HD.CDI (**C**) donors.

B,D) Plot of the entire dose range from the primary screen for mexiletine and **MexA2-5** analogues in hiPSC-CMs generated from LQT3 SCN5A F1473C (**B**) and HD.CDI (**D**) donors.

E-I) Blocking ratio ± SEM (1.0 = 100% inhibition; 0 = 0% inhibition) of I_{NaL} and I_{NaP} by mexiletine and **MexA2-5** analogues in *SCN5A* F1473C channels expressed in HEK cells by automated planar patch clamp recording.

J-N) Blocking ratio ± SEM (1.0 = 100% inhibition; 0 = 0% inhibition) of I_K by mexiletine and **MexA2-5** analogues in *hERG* channels expressed in CHO cells by automated planar patch clamp recording.

O-P) % inhibition of I_{NaL} (**O**) and I_{NaP} (**P**) was evaluated for each analogue at a single dose (EC_{80} for SCN5A F1473C from **Figure S2E-I**). Data points are % inhibition. Bar and error bars indicate the mean ± SEM.

Figure S3

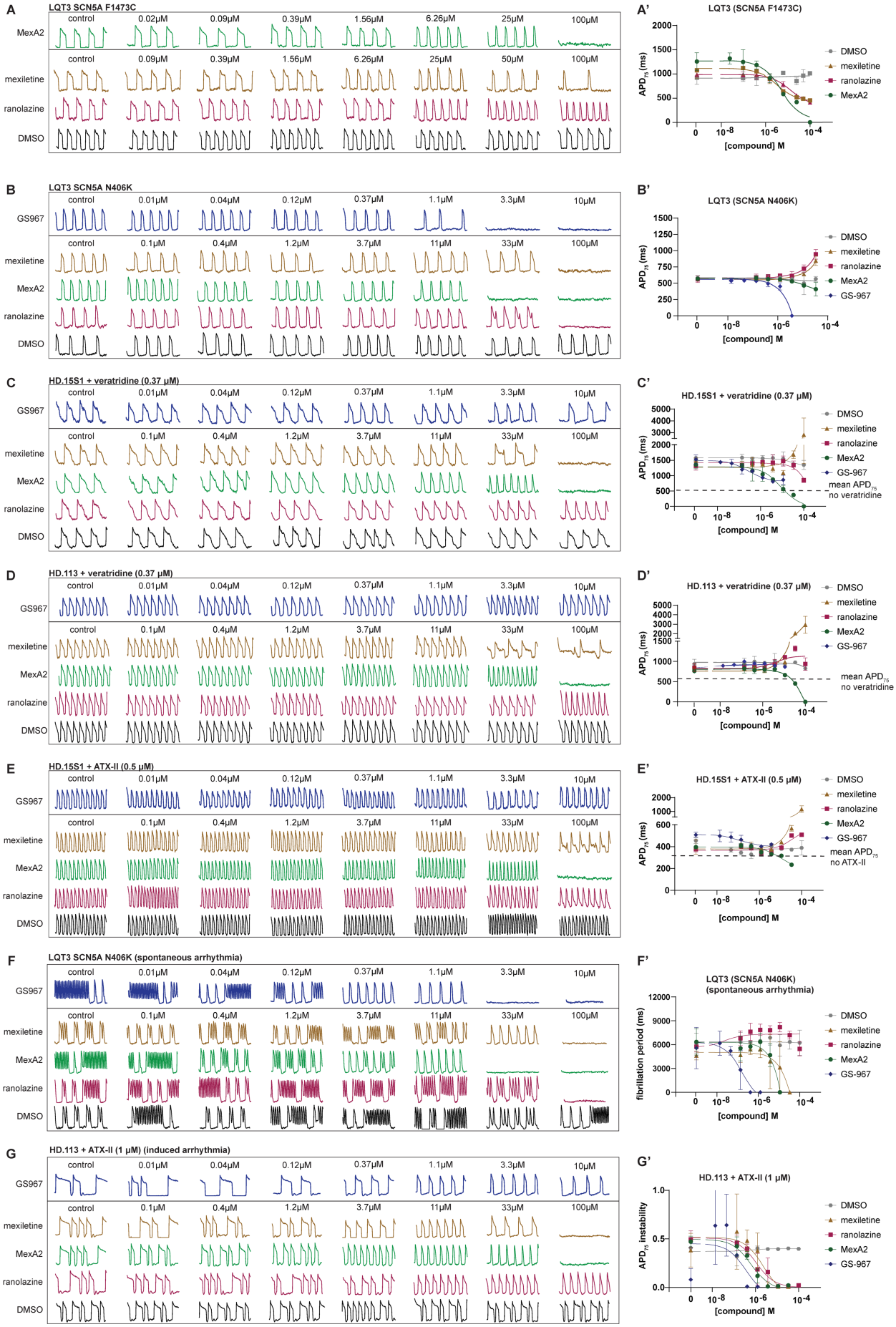
A
LQT3 SCN5A F1473C
control 0.02μM 0.09μM 0.39μM 1.56μM 6.26μM 25μM 100μM
MexA2
control 0.09μM 0.39μM 1.56μM 6.26μM 25μM 50μM 100μM
mexiletine
ranolazine
DMSO
A'
LQT3 (SCN5A F1473C)
APD75 (ms)
[compound] M
DMSO
mexiletine
ranolazine
MexA2
B
LQT3 SCN5A N406K
control 0.01μM 0.04μM 0.12μM 0.37μM 1.1μM 3.3μM 10μM
GS967
control 0.1μM 0.4μM 1.2μM 3.7μM 11μM 33μM 100μM
mexiletine
MexA2
ranolazine
DMSO
B'
LQT3 (SCN5A N406K)
GS-967
C
HD.15S1 + veratridine (0.37 μM)
C'
HD.15S1 + veratridine (0.37 μM)
mean APD75 no veratridine
D
HD.113 + veratridine (0.37 μM)
D'
HD.113 + veratridine (0.37 μM)
E
HD.15S1 + ATX-II (0.5 μM)
E'
HD.15S1 + ATX-II (0.5 μM)
mean APD75 no ATX-II
F
LQT3 SCN5A N406K (spontaneous arrhythmia)
F'
LQT3 (SCN5A N406K) (spontaneous arrhythmia)
fibrillation period (ms)
G
HD.113 + ATX-II (1 μM) (induced arrhythmia)
G'
HD.113 + ATX-II (1 μM)
APD75 instability

Figure S3. Effect of MexA2 and other I_{NaL} inhibitors in genetic and pharmacological models of LQT3. Related to Figure 4.

Dose response effect of **MexA2** (green), mexiletine (gold), ranolazine (purple), and GS-967 (blue) on LQT3 SCN5A F1473C (**A**), LQT3 SCN5A N406K (**B**), healthy donor HD.15S1 + veratridine (0.37 μM) (**C**), HD.113+vertridine (0.37 μM) (**D**), HD.15S1+ATX-II (0.5 μM) (**E**), LQT3-N406K spontaneous arrhythmia (**F**), and HD.113 +ATX-II induced arrhythmia (1 μM) (**G**). APD_{75} was used to measure the effect of **A**-**E**, APD_{90} was used for **F** and APD_{75} instability (APD_{75} standard deviation/APD_{75} mean) used for **G**. The data correspond to **Figure 4.** Data are represented as mean ± SEM for **A'-G'**.

Figure S4

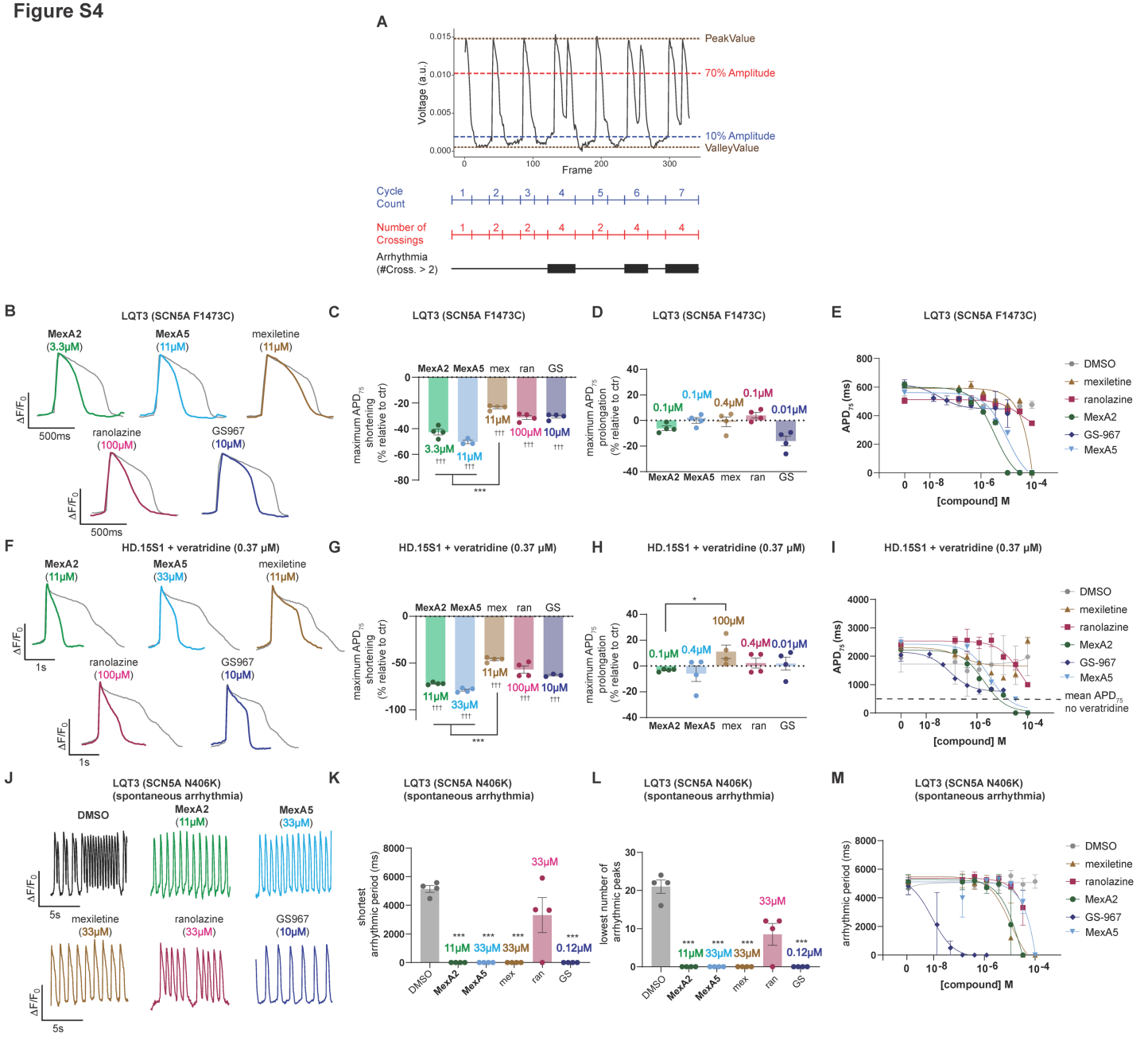

Figure S4. Effect of MexA5 on congenital and drug-induced LQT3. Related to Figure 4.

A) From each voltage trace, the baseline fluorescence (ValleyValue) and peak fluorescence (PeakValue) were identified. Beating cycles were counted as periods of time in which the voltage signal stayed above 10% of the amplitude (blue line). For each cycle, the number of crossings at 70% of the amplitude (red line) was counted (Number of Crossings). A cycle was flagged as arrhythmic if there were more than 2 crossings. The arrhythmic period is defined as the cumulative time of arrhythmic cycles (sum of the wide black bars above) and the number of arrhythmic peaks is the sum of the number of crossings of 70% amplitude divided by 2. Representative optical voltage recordings of action potentials from individual compounds at the lowest dose with maximum APD_{75} shortening (**B**), maximum APD_{75} shortening (**C**), prolongation (**D**) and dose response curve (**E**) for F1473C hiPSC-CMs. Representative optical voltage recordings of spontaneous action potentials from individual compounds at the lowest dose with maximum APD_{75} shortening (**F**), maximum APD_{75} shortening (**G**), prolongation (**H**) and dose response curve (**I**) for HD.15S1 hiPSC-CMs treated with 0.37 μM veratridine. Representative optical voltage recordings of action potential (**J**), shortest arrhythmic period (**K**), lowest number of arrhythmic peaks (**L**) attained by individual drugs (n= 3 wells) and a dose response curve (**M**) for LQT3 SCN5A

N406K hiPSC-CMs with spontaneous arrhythmia. Each trace (**A,E**) is an average normalized $\Delta F/F_0$ vs. time plot (33Hz) from multiple peaks in a well (n= 3-5 peaks). The grey lines (**A,E**) represent AP recording from respective control wells. APD_{75} shortening and prolongation times (ms) are represented as change from their respective control wells (n = 3-6 wells). Data are represented as mean ± SEM.

Supplementary Tables

Table S1. Summary of Electrophysiological parameters from automated planar patch clamp recording of SCN5A F1473C channel-transfected HEK cells. Related to Figure 2C and Figure S2E-N.

Compound ID	Peak Na^+ (I_{NaP}) Inhibition (μM)	Late Na^+ (I_{NaL}) Inhibition (μM)	$\Delta I_{NaP}/I_{NaL}$	hERG (I_{Kr}) Inhibition (μM)	$\Delta I_{Kr}/I_{NaL}$	Fold Change I_{NaL} Potency	Fold Change I_{NaL} Selectivity
mexiletine	182.8 ± 41.8	22.5 ± 4.4	8.3	53.7 ± 8.0	2.5	1.0	1.0
MexA1	20.6 ± 2.1	11.7 ± 0.8	1.8	8.0 ± 1.3	0.7	1.8	0.2
MexA2	34.2 ± 6.7	0.64 ± 0.04	53.4	22.9 ± 4.7	35.8	34.4	6.4
MexA3	20.1 ± 4.1	0.2 ± 0.05	100.5	6.2 ± 0.8	31.0	110.0	12.1
MexA4	41.1 ± 8.4	1.04 ± 0.03	39.5	37.5 ± 14.0	36.1	21.2	4.8
MexA5	25.8 ± 6.6	0.75 ± 0.6	34.4	27.6 ± 4.2	36.8	29.3	4.1

Table S2. Summary of Electrophysiological parameters from whole cell patch clamp recording of LQT3 SCN5A F1473C hiPSC-CMs. Related to Figure 2E-I.

Compound ID	Peak Na^+ (I_{NaP}) Inhibition (μM)	Late Na^+ (I_{NaL}) Inhibition (μM)	$\Delta I_{NaP}/I_{NaL}$	Fold Change I_{NaL} Potency	Fold Change I_{NaL} Selectivity
mexiletine	145	51	2.69	1	1
MexA2	> 102	1.7	60	30	22.3
MexA3	> 171	0.54	316	94.4	117
MexA4	> 200	1.8	111	28.3	41
MexA5	51.9	0.38	136	134	50